

Response of the quasi-biennial oscillation to a warming climate in global climate models

Journal:	<i>QJRM</i> S
Manuscript ID	QJ-19-0050
Wiley - Manuscript type:	Special Section QBO Modelling Intercomparison
Date Submitted by the Author:	07-Mar-2019
Complete List of Authors:	<p>Richter, Jadwiga; National Center for Atmospheric Research, Climate and Global Dynamics Laboratory Butchart, Neal; Met Office, Kawatani, Yoshio; Japan Agency for Marine-Earth Science and Technology, Research Institute for Global Change Bushell, Andrew; Met Office, Foundation Science Holt, Laura; NorthWest Research Associates Inc, Serva, Federico; National Research Council Anstey, James; Atmospheric, Oceanic and Planetary Physics, Department of Physics, University of Oxford, Simpson, Isla; National Center for Atmospheric Research, Osprey, Scott M.; Univ Oxford, Department of Physics Hamilton, Kevin; University of Hawaii at Manoa, International Pacific Research Center Braesicke, Peter; Karlsruhe Institute of Technology, Institute of Meteorology and Climate Research - Atmospheric Trace Gases and Remote Sensing Cagnazzo, Chiara; National Research Council Chen, Chih-Chieh; National Center for Atmospheric Research Garcia, Rolando; National Center for Atmospheric Research Gray, Lesley; University of Oxford Kerzenmacher, Tobias; Karlsruhe Institute of Technology, Institute of Meteorology and Climate Research - Atmospheric Trace Gases and Remote Sensing Lott, François; Ecole Normale Supérieure (ENS), LMD; McLandress, Charles; University of Toronto, Physics Naoe, Hiroaki; Meteorological Research Institute, Scinocca, John; Canadian Centre for Climate Modelling and Analysis Stockdale, Tim; European Centre for Medium Range Weather Forecasts Versick, Stefan; Karlsruhe Institute of Technology, Institute of Meteorology and Climate Research - Atmospheric Trace Gases and Remote Sensing Watanabe, Shingo; Japan Agency for Marine-Earth Science and Technology, Yoshida, Kohei; Meteorological Research Institute Yukimoto, Seiji; Meteorological Research Institute</p>
Keywords:	QBO, QBOi, Climate Change, Stratosphere < 4. Geophysical sphere, GCMs, Gravity Waves

1
2
3
4
5
6
7
8
9
10
11
12
13
14
15
16
17
18
19
20
21
22
23
24
25
26
27
28
29
30
31
32
33
34
35
36
37
38
39
40
41
42
43
44
45
46
47
48
49
50
51
52
53
54
55
56
57
58
59
60

Country Keywords:	United States, United Kingdom Of Great Britain And Northern Ireland, Canada, Japan, Germany



ORIGINAL ARTICLE**Journal Section**

Response of the quasi-biennial oscillation to a warming climate in global climate models

Jadwiga H. Richter¹ | Neal Butchart² | Yoshio Kawatani³ | Andrew C. Bushell⁴ | Laura Holt⁵ | Federico Serva⁶ | James Anstey⁷ | Isla R. Simpson¹ | Scott Osprey⁸ | Kevin Hamilton^{9,10} | Peter Braesicke¹¹ | Chiara Cagnazzo⁶ | Chih-Chieh Chen¹ | Rolando R. Garcia¹ | Lesley J. Gray⁸ | Tobias Kerzenmacher¹¹ | Francois Lott¹² | Charles McLandress^{8,13} | Hiroaki Naoe¹⁴ | John Scinocca⁷ | Timothy N. Stockdale¹⁵ | Stefan Versick¹¹ | Shingo Watanabe³ | Kohei Yoshida¹⁴ | Seiji Yukimoto¹⁴

¹Climate and Global Dynamics Laboratory,
National Center for Atmospheric Research,
Boulder, CO, 80307, USA

²Met Office Hadley Centre, Exeter, EX1
3PB, UK

³Japan Agency for Marine-Earth Science
and Technology, Yokohama, Japan

⁴Met Office, Exeter, UK

⁵North West Research Associates (NWRA),
Boulder, USA

⁶Institute of Marine Sciences, National
Research Council (ISMAR-CNR), Rome,
Italy

⁷Canadian Centre for Climate Modelling
and Analysis (CCCma), Victoria, Canada

⁸National Centre for Atmospheric Science
(NCAS), University of Oxford, Oxford, UK

⁹International Pacific Research Center,
University of Hawaii, Honolulu, USA

¹⁰International Pacific Research Center
(IPRC), Honolulu, USA

¹¹Karlsruher Institut für Technologie (KIT),
Karlsruhe, Germany

¹²Laboratoire de Météorologie Dynamique
(LMD), Paris, France

¹³University of Toronto, Toronto, Canada

¹⁴Meteorological Research Institute (MRI),
Tsukuba, Japan

¹⁵European Centre for Medium-Range
Weather Forecasts (ECMWF)

Correspondence
Jadwiga H. Richter, Climate and Global
Dynamics Laboratory, National Center for
Atmospheric Research, Boulder, CO, 80307,
USA
Email: jrichter@ucar.edu

Funding information

We compare the response of the quasi-biennial oscillation (QBO) to a warming climate in eleven atmosphere general circulation models that performed time-slice simulations for present-day, doubled, and quadrupled CO₂ climates. No consistency was found among the models for the QBO period response, with the period decreasing by eight months in some models and lengthening by up to thirteen months in others in the doubled CO₂ simulations. In the quadrupled CO₂ simulations a reduction in QBO period of 14 months was found in some models, whereas in several others the tropical oscillation no longer resembled the present day QBO, although could still be identified. In contrast, all the models projected a decrease in the QBO amplitude in a warmer climate with the largest relative decrease near 60 hPa. In simulations with doubled and quadrupled CO₂ the multi-model mean QBO amplitudes decreased by 36% and 51%, respectively. Across the models the differences in the QBO period response were found most strongly related to how the gravity wave momentum flux entering the stratosphere and tropical vertical residual velocity responded to the increases in CO₂ amounts. Likewise it was found that the robust decrease in QBO amplitudes was correlated across the models to changes in vertical residual velocity, parameterized gravity wave momentum fluxes, and to some degree the resolved upward wave flux. We argue that uncertainty in the repre-

sensation of the parameterized gravity waves is the mostly likely cause of the spread among the eleven models in the QBO's response to climate change.

KEYWORDS

QBO, QBOi, Climate Change, GCMs, Stratosphere, Gravity Waves

1 | INTRODUCTION

The quasi-biennial oscillation (QBO) is the most prominent feature of the circulation of the equatorial stratosphere. Alternating descending easterly and westerly shear zones have been observed consistently near the equator between 100 and 10 hPa since 1953 with an average period of 28 months (Naujokat, 1986; Baldwin et al., 2001). The QBO is understood to be maintained largely by momentum deposition from upward propagating large scale Kelvin and mixed-Rossby gravity waves, gravity waves with horizontal scales of tens to thousands of kilometers, and vertical advection. Variability in these three forcing terms contributes to the variable period of the QBO, which ranges from 22 to 34 months in the observational record (Baldwin et al., 2001). Although the basic mechanism of QBO formation is well understood, many general circulation models (GCMs) have difficulty reproducing this oscillation. For most GCMs, the ability to reproduce the QBO is strongly dependent on the parameters of the gravity wave (GW) parameterization, which are poorly constrained by observations, and often tuned to obtain the correct present-day period and amplitude of the oscillation, and hence are a very large source of uncertainty in modeling of the QBO.

Several studies have addressed the question of how the QBO is likely to change in the future, however the findings have been inconclusive, primarily due to the large uncertainty associated with parameterized gravity waves. The model study of the QBO changes in a warm climate by Giorgetta and Doege (2005) showed that the QBO period decreases in doubled CO₂ simulations from 29 to 26, 22, and 17 months in experiments in which gravity wave source remain the same, and increased by 10%, and then 20% respectively. The QBO period reduction in the warming climate resulted from both the prescribed increase of wave sources and a simulated decrease in the tropical upwelling though the latter is not in agreement with most model projections of increased tropical upwelling in a warmer climate (Butchart et al., 2006). Kawatani et al. (2011) used a model without parameterized non-orographic gravity waves and found the effect

1
2 51 of enhanced mean tropical upwelling in a warming climate overwhelms the counteracting influence from strengthened
3
4 52 wave fluxes. Consequently, the amplitude of the QBO becomes smaller, especially in the lower stratosphere and the
5
6 53 period becomes longer. Watanabe and Kawatani (2012) also projected that the QBO will lengthen and the amplitude
7
8 54 become smaller in a warming climate but in a model in which sources of parameterized gravity waves remained fixed,
9
10 55 and the change in the QBO resulted from changes to the vertical residual velocity. Kawatani and Hamilton (2013)
11
12 56 analyzed four Coupled Model Intercomparison Project phase 5 (CMIP5) models that could simulate a spontaneous QBO.
13
14 57 They showed that a long term reduction in the QBO amplitude in the lower stratosphere is robust in all four models and
15
16 58 they also found this clearly in observations at 70 hPa from 1953 to 2012. On the other hand, the four models produced
17
18 59 different projections of the QBO period changes, while the 60-year observational record showed no significant trends
19
20 60 in QBO period. Schirber et al. (2015) found that the response of the amplitude and period of the QBO to a warming
21
22 61 climate was dependent on the configuration of gravity wave parameterizations in their model, and hence their findings
23
24 62 were inconclusive.

25
26 63 The lack of agreement among these earlier studies on how the QBO may change in the future and the need to under-
27
28 64 stand how assumptions in gravity wave parameterizations influence these findings helped motivate the Stratosphere-
29
30 65 troposphere Processes And their Role in Climate (SPARC) Quasi-Biennial Oscillation initiative (QBOi) designed to
31
32 66 improve the fidelity of tropical stratosphere variability in present day GCMs (Butchart et al., 2018). For phase 1 of
33
34 67 QBOi, five experiments were designed in combination to: evaluate the ability of GCMs to represent the QBO in present
35
36 68 day climate (QBOi Experiments 1 and 2), examine the response of the QBO under climate-change forcings in various
37
38 69 GCMs (QBOi Experiments 2, 3, and 4), and evaluate the ability of GCMs to predict the QBO when initialized with
39
40 70 observations (QBOi Experiments 5 and 5a). Seventeen GCMs participated in phase 1 of QBOi and carried out some or
41
42 71 all of the experiments (Butchart et al., 2018). In a companion paper, Bushell et al. (2019) describe the characteristics and
43
44 72 forcing of the QBO in present day climate among these models. In this paper we discuss the response of the QBO in a
45
46 73 doubled and quadrupled CO₂ climate among eleven GCMs that participated in Experiments 2, 3, and 4. We examine
47
48 74 here the robustness of changes in the QBO and changes in QBO forcings among these models, as well as discuss the
49
50 75 factors that contribute to the largest uncertainty in the response of the QBO. The details of changes in the momentum
51
52 76 budget in the three experiments will be reported in a follow-up publication. The paper is organized as follows: the
53
54 77 models, experimental set-up, and changes to the mean state of the stratosphere are described in section 2. Section 3
55
56 78 describes changes to the QBO. Section 4 discusses changes in QBO forcing terms, and section 5 presents summary and
57
58 79 conclusions.

2 | MODELS, EXPERIMENTAL SETUP, AND MEAN CLIMATE

2.1 | Models

We utilize here output from eleven atmosphere only GCMs that participated in QBOi and performed Experiments 2, 3 and 4. The participating models, GW parametrization specifications, and years of simulation in each experiment are listed in Table 1. For references to model descriptions, comparison of vertical/horizontal resolutions, time steps, convection parameterizations, and numerical advection schemes among the models, the reader is referred to Butchart et al. (2018).

The majority of the QBOi models have fixed gravity wave sources, meaning that the spectrum of GWs launched at the source level does not change as the climate changes and is fixed (as are all other model characteristics) between Experiments 2, 3, and 4. The only exception to that are models using the Hines (1997a,b) scheme (ECHAM5sh, EMAC, MIROC-ESM, and MRI-ESM2), for which the GW wavenumber spectrum, and in particular the so-called "cutoff wavenumber" depends on the buoyancy frequency at the source level, which varies between the experiments, resulting in a change in total momentum flux at source level. Four of the eleven models (60LCAM5, CESM1(WACCM5-110L), LMDz6, and UMGA7gws) have gravity wave source parameterizations that link the properties of non-orographic GWs to the properties of their sources in the troposphere (described in more detail in Section 4.2). UMGA7 and UMGA7gws differ only in the representation of parameterized gravity waves, with UMGA7 including a fixed and UMGA7gws including a variable GW source spectrum. One of the models, MIROC-AGCM-LL, is able to reproduce the QBO without parameterizing non-orographic GWs. The cumulus parameterization in MIROC-AGCM-LL is based on the method of Arakawa and Schubert (1974), with a relative humidity limit method. Both this method and high vertical resolution enable the MIROC-AGCM-LL to simulate the QBO without a GW parameterization.

2.2 | Experimental Setup

The simulation setup for all models followed the QBOi protocol (Butchart et al., 2018):

- Experiment 2 (hereafter 'Exp 2') is a present-day timeslice experiment in which a repeated annual cycle of sea surface temperatures (SSTs) and sea-ice is employed, and 2002 external forcings.

TABLE 1 Models participating in QBOi Experiments 2, 3 and 4 and specifications of their non-oro-graphic gravity wave parameterizations (NOGW Param), GW source parameterization (NOGW Source), GW Source Level (GW SL), and number of years in Exp 2, 3, and 4. Some models performed several ensembles indicated by the number 'x' in the Yrs columns. AGCM3-CMAM did not perform Exp 4. Non-oro-graphic GW parameterizations are abbreviated as follows: Hines (1997a,b) [Hi]; Warner and McIntyre (1999) [WM]; Lindzen (1981) [Li]; Lott et al. (2012) [Lo].

Model	NOGW Param	NOGW Source	GW SL	Yrs Exp 2	Yrs Exp 3	Yrs Exp 4
60LCAM5	[Li]	Richter et al. (2010)	Variable	3x38	38	38
AGCM3-CMAM	[WM]	Fixed	90 hPa	3x31	3x31	0
CESM1(WACCM5-110L)	[Li]	Richter et al. (2010)	Variable	33, 2x35	31	31
ECHAM5sh	[Hi]	Fixed	600 hPa	30	30	30
EMAC	[Hi]	Fixed	643 hPa	106	106	106
LMDz6	[Lo]	Lott and Guez (2013)	500 hPa	70	70	70
MIROC-AGCM-LL	None	N/A	N/A	3x30	3x30	3x30
MIROC-ESM	[Hi]	Fixed	657 hPa	100	3x30	3x30
MRI-ESM2	[Hi]	Fixed	Surface	30	30	30
UMGA7	[WM]	Fixed	4 km	105	105	105
UMGA7gws	[WM]	Bushell et al. (2015)	4 km	105	105	105

- Experiment 3 (hereafter 'Exp 3') is the same as Exp 2 but with a 2 K temperature perturbation added uniformly to the SSTs and double the CO₂ concentration of Exp 2.
- Experiment 4 (hereafter 'Exp 4') is the same as Exp 2 but with a 4 K temperature perturbation added uniformly to the SSTs and quadruple the CO₂ concentration of Exp 2.

Full details of the QBOi Experiments can be found in Butchart et al. (2018).

2.3 | Mean Climate

Figure 1 shows the multi-model mean change in the annual- and zonal-mean zonal wind and temperature as a function of latitude and height for Exp 3 and 4 relative to Exp 2. All models are given equal weight in the presented multi-model means. Consistent with the basic radiative effects of CO₂ and increased SSTs, the temperature increases in the troposphere and decreases in the stratosphere in Exp 3 and Exp 4 as compared to Exp 2, both for the multi-model mean (Figure 1a, b) and also for each of the models (not shown). The multi-model response of the zonal mean zonal wind

to increased CO₂ concentration and SSTs show poleward shifting and upward expansion of the mid-latitude jets in the troposphere and strengthening of the extra-tropical jets throughout the stratosphere, especially in the Southern Hemisphere (Figure 1c, d), broadly similar to previous studies (Barnes and Polvani, 2013; Shepherd and McLandress, 2011; Simpson et al., 2014).

In the tropical troposphere, temperature and static stability increase, on average, in Exp 3 and 4 as compared to Exp 2 (Figure 2), while in the lower stratosphere (90 to 40 hPa) temperature changes are small and not significant compared to the inter model spread in either Exp 3 or 4. All the models agree on the warming in the troposphere and cooling of the stratosphere, but the exact altitude where they transition between this warming and cooling varies across models (not shown). The decrease in static stability in the equatorial lower stratosphere in Exp 3 and 4 relative to Exp 2, shown in Figure 2b, is robust across models.

3 | QBO

Figure 3 shows a 20-year time series of near-equatorial zonal mean winds for Exp 2, 3, and 4. For current SSTs and amounts of CO₂ (Exp 2) the left hand panels confirm that all the models capture the characteristic features of the observed QBO, including alternating layers of descending easterlies and westerlies in the stratosphere. There is still a spread among models in terms of QBO period and amplitude as described in Bushell et al. (2019). Figure 4 shows the results of the same experiments but with the mean seasonal cycle subtracted from the zonal mean winds. After removing the seasonal cycle, the vertical structures of the QBOs in Exp 2 in the various models more closely resemble each other, and regular downward phase progression all the way to the tropopause in each model is quite apparent.

As SSTs increase and the amount of CO₂ is doubled (Exp 3, middle column Figure 3), then quadrupled (Exp 4, right-most column Figure 3), the characteristic QBO signal weakens in all models in the raw time series, and in some cases is no longer discernible for Exp 4 (e.g. ECHAM5sh). However, if the seasonal cycle is subtracted from the zonal mean winds (Figure 4), then a signal of descending layers of eastward and westward wind shear can be identified in all models for the three experiments as confirmed by the lag-correlations (see below for details) shown in Figure 5 for Exp 4.

A robust and systematic decrease in the QBO amplitude with increasing SSTs and CO₂ concentration can be seen in Figures 3 and 4. The sign of change in the QBO period, on the other hand is model dependent, with some models

projecting a decrease, some projecting a lengthening, and others predicting little change. These differences in behaviour are consistent across Exp 3 and Exp 4 and do not appear to be connected to any particular aspect or combination of aspects of model formulation and in particular any of those cataloged in Table 1. However, we note that given the small size of the multi-model ensemble (11 models) as compared to the number of differences in model formulation, it can be difficult to robustly identify any aspect of model formulation as being responsible for the different responses in QBO period.

We quantify the changes in QBO period and amplitude in Exp 3 and Exp 4 building on metrics presented in Bushell et al. (2019) for QBOi Experiment 1 (present-day forcings with varying SSTs), and employ additional diagnostics that help elucidate QBO characteristics in simulations for which the oscillation is more erratic than the present-day QBO.

3.1 | QBO Periods:

We derive QBO periods using three methods, defined as follows:

- ‘QBO Transition Times (TT)’: following Bushell et al. (2019), zero wind transitions from westward to eastward winds are identified at a reference level of 10 hPa and used to define QBO cycles. Wind transitions are identified in an equatorial averaged zonal mean zonal wind time series between 5°S to 5°N at 10 hPa which was smoothed using a 5-month centered running mean. A QBO period and amplitude for each QBO cycle is identified from the zonal mean wind time series between individual transition points. Using this method, standard deviation of the periods and amplitudes can then be derived from these distributions in addition to the mean.
- ‘Fast Fourier Transform (FFT)’: analysis was performed on a 5°S to 5°N averaged zonal mean zonal wind deaseasonalized time series which was padded at the end with zeros to 10 times the length of original time series to increase the spectral resolution. FFT analysis was performed at levels between 50 and 10 hPa. In Exp 2, the FFT spectra typically have one dominant peak, and the Fourier amplitude is highest at exactly the same period at all levels between 50 and 10 hPa. In Exp 3 and Exp 4 the FFT spectra in many models no longer have a well-defined peak and often have several peaks of similar amplitude. In addition, in some simulations the dominant QBO period varies with altitude (not shown). A range of QBO periods is provided for simulations in which the dominant FFT period between 50 and 10 hPa varies by more than a month.
- ‘Lag correlations (LAG)’: The correlation of the time series of equatorial zonal mean wind at 10 hPa with the

corresponding lagged time series (i.e. at $t \pm lag$) at each level confirms the presence of an oscillation for all models, with increasing phase lag on descending through the stratosphere (see Figure 5 for Exp 4). In most models a well defined mean period can be deduced from the correlations [e.g. CESM1(WACCM5-110L)] while in other models (e.g. ECHAM5sh and UMGA7gws) the point of maximum correlation is followed, or preceded, by more than one local maximum anti-correlation. The larger of these local maxima, as indicated by the black vertical lines in the figure is used to define the mean period used in the rest of the paper. The absence of an unambiguous period in the lag-correlations is consistent with the less clear QBO signals in Figures 4 and 5 and the absence of a well defined peak in the power spectra.

The findings from the above diagnostics are summarized in Table 2. An oscillation can be identified in all the simulations, however the changed nature of the oscillations in several models in Exp 3 and Exp 4 are reflected by a discrepancy in the mean period derived by the three methods and/or a range of periods between 50 and 10 hPa. These include ECHAM5sh in Exp 3, and ECHAM5sh, MIROC-ESM, and UMGA7gws in Exp 4.

Changes in QBO periods derived using the TT method are visualized in Figure 6. Using this period-derivation method allows for visualizing the range of QBO periods in addition to the mean and standard deviation. Three models (60LCAM5, CESM1(WACCM-110L), and MRI-ESM2) predict much shorter QBO periods with increasing SSTs/CO₂ in Exp 3 and Exp 4 with predicted mean periods between 15 and 18 months in Exp 4. ECHAM5sh, EMAC, UMGA7, UMGA7gws predict no significant change in the mean QBO period in Exp 3, whereas AGCM3-CMAM, LMDz6, MIROC-AGCM-LL, and MIROC-ESM project lengthening of the QBO period. In Exp 4, LMDz6, MIROC-AGCM-LL, and UMGA7gws predict statistically significant lengthening of the QBO ranging from 3 to 10 months relative to present day. ECHAM5sh, EMAC, MIROC-ESM, and UMGA7 predict no significant change in QBO period in Exp 4. In a multi-model mean (Table 2), the QBO period does not change between the experiments, however as seen from Figure 6 that is not representative of most individual models. Figure 6 and standard deviations in Table 2 for individual models and multi-model mean show that in general the range and variability of simulated QBO periods increases in the warming climate, especially in Exp 4. The more variable nature of the near-equatorial oscillation is also revealed by the FFT analysis, which has shown that spectra tend to have multiple peaks, especially in Exp 4, whereas most models had very well defined spectral peaks in Exp 2 (not shown).

TABLE 2 Summary of estimates of QBO periods in Exp 2, 3, 4 using three different methods: TT, FFT, and LAG. For the TT method standard deviation is denoted after the \pm sign. For simulations in which the dominant period varies by more than 1 month between 50 and 10 hPa a range of dominant periods is specified. Simulations for which the TT and LAG methods of period estimation do not agree to within 4 months are marked with a *. Period values in Exp 3 and Exp 4 derived using the TT method that are statistically different from Exp 2 at the 95 % level as defined by the Student t-test for unequal sized distributions are bolded. ** indicates that for ECHAM5sh transition times were calculated at 15 hPa, as the oscillation was poorly defined at 10 hPa and a clear period was difficult to obtain. The multi-model mean is listed in the bottom row of the table. For periods derived using the FFT method in Exp 3 and Exp 4 the multi-model mean is not defined (ND) due to the range of dominant periods for some of the models.

Model	Exp 2			Exp 3			Exp 4		
	TT	FFT	LAG	TT	FFT	LAG	TT	FFT	LAG
60LCAM5	24.3 \pm 1.6	24.3	23	18.5\pm5.2	20.3	18	14.2\pm3.6	14.8	16
AGCM3-CMAM	26.9 \pm 1.8	27.1	26	41.2\pm8.0	40.0-53.0	39	N/A	N/A	N/A
CESM1(WACCM5-110L)	27.6 \pm 2.4	27.5	28	19.7\pm1.3	19.8	20	14.0\pm2.0	14.5	14
ECHAM5sh	26.5 \pm 1.8	26.9	26	27.0** \pm 5.7	23.4-39.1	32*	32.2 \pm 13.6	25.5-44	32
EMAC	26.5 \pm 2.0	26.7	26	27.7 \pm 3.5	27.1	28	27.6 \pm 4.0	27.8	28
LMDz6	27.3 \pm 2.7	27.3	26	33.0\pm4.8	34.7	32	35.9\pm17.7	32.1	36
MIROC-AGCM-LL	19.2 \pm 1.5	19.3	18	20.7\pm2.0	20.8	20	21.9\pm4.5	23.3	21
MIROC-ESM	24.1 \pm 2.6	24.1	24	26.6\pm3.0	25.4	26	22.6 \pm 8.8	26.1 - 34.6	26
MRI-ESM2	22.5 \pm 3.6	22.5	22	15.6\pm4.1	19.7	15	14.0\pm3.9	17.5	13
UMGA7	26.0 \pm 2.6	26.9	26	26.0 \pm 4.6	26.6	26	28.7 \pm 8.6	30.3	29
UMGA7gws	23.9 \pm 2.1	23.9	24	24.2 \pm 5.2	25.3	28	22.1 \pm 9.5	32.7-94.0	34*
Multi-Model Mean	25.0 \pm 2.5	25.1	25	25.5\pm4.3	ND	26	23.3\pm7.6	ND	25

3.2 | QBO Amplitudes

QBO amplitudes are derived using two methods:

- ‘TT’: following from the QBO transition times method for calculating QBO periods described in previous section. Amplitudes associated with each phase at 10 hPa were estimated by taking the maximum or minimum value within the identified time period between zero transitions in the original timeseries with higher frequency variability reduced through a 5-month centered binomial smoothing following Bushell et al. (2019).
- ‘Dunkerton and Delisi (DD)’: Dunkerton and Delisi (1985) observed that, when most of the variability in the monthly mean equatorial winds results from the QBO, the mean amplitude of the oscillation can be approximated by $\sqrt{2}\sigma$, where σ is the standard deviation of the deseasonalized time series of the monthly mean eastward winds. This allows the mean amplitudes, though not the distribution of amplitudes, to be easily calculated as functions of

latitude and height and these agree well with the mean amplitudes obtained from the TT method for simulations with well defined QBOs. Furthermore, even if clearly defined QBO cycles are not present, the diagnostic can still be usefully interpreted as a general quantitative measure of the amount of variability present.

Amplitudes derived using the above methods at 10 hPa are summarized in Table 3. We chose not to use the FFT method to derive QBO amplitudes due to the change in the nature of the QBO towards more than one dominant spectral component in the warming climate. In present day, amplitudes derived from the peak in the Fourier spectrum are in good agreement with the TT and DD method, however due to the multiple peaks in the spectra in Exp 4, FFT based amplitudes largely underestimate the amplitudes derived from the other methods.

For all Exp 2 and nearly all Exp 3 and 4 models the highest estimate of the mean amplitude is obtained from the DD method, which often exceeds the mean amplitude derived from the TT method by more than one standard deviation of the TT derived amplitudes. Partially this is due to Bushell et al. (2019)'s use of binomial smoothing (see above) which, as well as damping high frequency variations, will damp the amplitude of the QBO—binomial smoothing is used here merely for consistency with Bushell et al. (2019). Models and experiments for which the DD method does not give the highest estimate of the mean amplitude are ECHAM5sh (Exp 3 & 4) and LMDz6 (Exp 4). In these simulations there is significant ambiguity when identifying individual QBO cycles (cf. Figure 3) and it is likely that the QBO phase transition point algorithm combines some cycles with the consequence of excluding some of the smaller local easterly and westerly maxima, hence giving rise to a spuriously high estimate for the mean amplitude.

The bottom panel in Figure 6 shows changes in the distribution of QBO amplitudes at 10 hPa calculated using the TT method. Although there is a wide spread in QBO amplitudes among the models for Exp 2, most models show a decrease in mean amplitudes for Exp 3 and Exp 4 in comparison to Exp 2, with the exception of MIROC-AGCM-LL with a slightly larger mean amplitude in Exp 3 than in Exp 2. The multi-model mean (see Table 3) also shows a consistent decrease of QBO amplitude with warming climate using both the TT and DD methods. The range of amplitudes in Exp 3 and Exp 4 increases in most models, as also demonstrated by the increase in the standard deviation of the amplitudes of individual models and multi-model mean.

Figure 7 shows the separation of QBO amplitude at 10 hPa into the westerly and easterly phases based on the TT method. On average there is little change in the amplitude of the westerly phase with a decrease in some models and an increase in others. In contrast the amplitude of the easterly phase decreases in all models and, on average, decreases from 30 ms^{-1} in Exp 2 to 20 ms^{-1} in Exp 4. Hence, there is a decrease in the asymmetry between the amplitude of

TABLE 3 Summary of estimates of QBO amplitudes in Exp 2, 3, 4 using two different methods: TT and DD. For the TT method standard deviation is denoted after the \pm sign. Ratio of westerly to easterly amplitudes calculated from the TT method is listed in the 'W/E' column. Amplitude values for individual models in Exp 3 and Exp 4 derived using the TT method that are statistically different from Exp 2 at the 95 % level as defined by the Student t-test for unequal sized distributions are in bold.

Model	Exp 2			Exp 3			Exp 4		
	TT	DD	W/E	TT	DD	W/E	TT	DD	W/E
60LCAM5	23.0 \pm 2.9	24.6	0.68	21.4 \pm 4.8	24.6	0.71	18.7\pm3.9	20.5	0.69
AGCM3-CMAM	22.4 \pm 0.9	24.5	0.36	20.7\pm3.3	21.8	0.41	N/A	N/A	N/A
CESM1(WACCM5-110L)	26.0 \pm 1.3	28.9	0.43	24.8\pm1.4	27.8	0.47	20.8\pm2.3	24.4	0.61
ECHAM5sh	27.8 \pm 2.6	30.6	0.89	16.5\pm10.9	23.4	1.07	21.1\pm3.3	14.4	1.49
EMAC	25.7 \pm 1.4	28.0	0.65	24.9\pm1.4	26.6	0.69	22.3\pm1.7	23.0	0.78
LMDz6	22.3\pm1.4	23.5	0.65	19.9\pm1.6	19.8	0.72	16.2\pm3.1	15.4	1.02
MIROC-AGCM-LL	19.7 \pm 0.8	20.9	0.61	20.0 \pm 0.9	21.0	0.61	17.1\pm2.6	17.5	0.73
MIROC-ESM	22.8 \pm 1.4	24.2	0.47	21.1\pm1.9	21.4	0.56	16.5\pm4.1	18.6	0.77
MRI-ESM2	16.6 \pm 3.7	18.8	0.59	13.3\pm2.4	14.1	0.71	13.4\pm2.7	11.1	0.96
UMGA7	28.7 \pm 0.9	32.1	0.6	24.6\pm2.6	26.6	0.70	19.7\pm4.1	21.0	0.75
UMGA7gws	23.8 \pm 1.2	25.8	0.56	19.6\pm3.7	20.0	0.66	13.1\pm3.8	10.5	0.73
Multi-model Mean	23.5\pm1.7	25.6	0.6	20.6\pm3.2	22.5	0.7	17.9\pm3.1	17.6	0.85

easterly and westerly phases in the multi-model mean response to a warming climate (Figure 7c).

In most models, in Exp 2 the QBO amplitude peaks at the Equator near 10 hPa (Figure 8), then decreases in both amplitude and width on descending into the lower stratosphere (Bushell et al., 2019). In Exp 3 and Exp 4 there is a robust decrease in the amplitude relative to Exp 2 in all models at all levels above 80 hPa. At each level the decrease is more or less uniform across the full width of the QBO but with a hint of a slightly stronger decrease in the Southern Hemisphere (Figure 8). At 10 hPa the amplitude decrease is strongest away from the local maximum in QBO amplitude at the equator. The percentage decrease in QBO amplitude in the multi-model mean declines with height between ~60 hPa and 10 hPa: from 36% in Exp 3 and 51% in Exp 4 at 60 hPa to 12% and 31%, respectively at 10 hPa. Although the QBO amplitude decrease increases with the amount of CO₂, it does not scale linearly.

4 | CHANGES IN QBO FORCING TERMS

In the present climate there is a balance between momentum tendencies from vertical and meridional advection and resolved and parameterized gravity waves that produce an oscillation in the tropics with a mean period of 28 months,

and an amplitude of $\sim 24 \text{ m s}^{-1}$ at the peak of the oscillation at 15 hPa. The tendencies driving the QBO can be described using the Transformed Eulerian Mean (TEM) zonal wind equation (Andrews et al., 1987):

$$\bar{u}_t = -\bar{v}^* \left[(a \cos \phi)^{-1} (\bar{u} \cos \phi)_\phi - f \right] - \bar{w}^* \bar{u}_z + \bar{X} + (\rho_0 a \cos \phi)^{-1} \nabla \cdot \mathbf{F} \quad (1)$$

where \bar{u} is the zonal-mean zonal wind, a is the radius of the earth, ϕ is the latitude, \bar{v}^* and \bar{w}^* are the residual meridional and vertical velocities. The first term on the right-hand side of (1) is the meridional advection and the Coriolis torque (f is the Coriolis parameter) which is typically quite small, the second term is the vertical advection, \bar{X} is the gravity wave drag and the last term is the Eliassen-Palm flux divergence from resolved waves. Definition of the EP flux vector can be found in Andrews et al. (1987, pp. 127-130) and precise details of how these diagnostics were calculated for the QBOi archive are given by Butchart et al. (2018).

In a warming climate, each of the tendencies in (1) are likely to respond differently and, as the tendency terms themselves are dependent on the mean wind which they alter, the prediction of how the QBO responds to a warming climate is not straightforward. In the subsequent four subsections we consider how vertical advection, EP flux divergence, and momentum flux from parameterized GWs change in Exp 3 and Exp 4, and then analyze how these changes correlate with the projected changes in QBO period and amplitude.

4.1 | Vertical Advection

Vertical advection, proportional to the vertical wind shear and the vertical residual velocity or upwelling, acts to slow down the downward propagation of QBO easterly shear zones (e.g. Saravanan, 1990; Dunkerton, 1991). An increase (decrease) in upwelling would hence act to lengthen (shorten) the QBO cycle, all else being equal. There is observational evidence that the Brewer-Dobson circulation, and hence tropical upwelling have been increasing since 1980 (Fu et al., 2015). Nearly all modeling studies also agree that a warming climate would lead to increased tropical upwelling (e.g. Butchart et al., 2006; Lin and Waugh, 2013), though there is some spread in the projected magnitude of the increase (e.g. Austin et al., 2003). This speeding-up of the Brewer Dobson circulation comes from increased gravity wave drag resulting from changes in the subtropical jets (Butchart et al., 2010) and increased extra-tropical EP flux divergence. The increased EP flux divergence results from changes in the thermal structure of the atmosphere in a warming climate

1
2 266 and also changes in tropospheric sources of upward propagating waves (e.g. Mclandress and Shepherd, 2009; Winter
3
4 267 and Bourqui, 2010).

5 268 Figure 9 shows the change in the multi-model mean as well as the individual model estimates of residual vertical
6
7 269 velocity, \bar{w}^* , in Exp 3 and Exp 4. Figure 9a shows that, on average, there is an overall increase in \bar{w}^* between 100 and 5
8
9 270 hPa and there is an upward shift in the climatological vertical structure of \bar{w}^* , with the minimum in the multi-model
10
11 271 mean shifting from 60 hPa in Exp 2 to 50 hPa in Exp 4. The upward shift in \bar{w}^* is consistent with the upward shift of
12
13 272 the climatological cold point tropopause (Figure 2b) and upward expansion of the subtropical jet leading to an upward
14
15 273 shift of the shallow branch of the Brewer-Dobson circulation (Garcia and Randel, 2008). In Exp 3 and 4 \bar{w}^* increases
16
17 274 in all models at most altitudes in the 100 to 20 hPa range, with a few models not showing much change above 50 hPa
18
19 275 (Figures 9b, c). Averaged between 100 and 50 hPa, the near-equatorial residual vertical velocity increases relative to
20
21 276 Exp 2 by 10-38% for Exp 3, and by 15-75% for Exp 4. The largest increases occur roughly near the altitude where \bar{w}^* is a
22
23 277 minimum between 80 and 50 hPa, and are most pronounced in AGCM3-CMAM, ECHAM5sh, and EMAC in Exp 3 and
24
25 278 ECHAM5sh and EMAC in Exp 4.

26 279 **4.2 | Gravity Waves**

27
28 280 Gravity wave drag from parameterized GWs provides at least 50% of the forcing of the QBO in the QBOi models, except
29
30 281 for in MIROC-AGCM-LL, which doesn't employ a GW parameterization (Bushell et al., 2019). In the real atmosphere,
31
32 282 GW momentum flux entering the stratosphere can change as a result of changes in tropospheric gravity wave sources,
33
34 283 and changes in their propagation due to different background wind and temperature profiles. As the majority of QBOi
35
36 284 models uses fixed GW sources (Table 1), the spectrum of waves launched at the source level will be exactly the same
37
38 285 in Exp 2, 3, and 4, except for a change in the total momentum flux in models utilizing the Hines (1997a,b) scheme
39
40 286 (ECHAM5sh, EMAC, MIROC-ESM, and MRI-ESM2) due to the change in buoyancy frequency at the launch level in Exp 3
41
42 287 and 4 (cf. Figure 2). The launch levels of GWs vary from the surface (MRI-ESM2) to 90 hPa (AGCM3-CMAM), hence,
43
44 288 apart from AGCM3-CMAM, the parameterized GW spectrum reaching the stratosphere is affected by propagation
45
46 289 through the troposphere and consequentially is likely to be different in Exp 3 and Exp 4. For MRI-ESM2, in particular,
47
48 290 the source spectrum is affected by a 8(18)% increase in Exp 3 (Exp 4) in buoyancy frequency at the surface. ECHAM5sh,
49
50 291 EMAC, and MIROC-ESM, also using the Hines (1997a,b) scheme, launch GWs near 600 hPa, at a level at which buoyancy
51
52 292 frequency changes between Exp 3 and Exp 4 and Exp 2 are small, hence the GW source spectra are very similar in
53
54
55

all experiments. Vertical profiles of eastward and westward GW momentum flux averaged between 10°S and 10°N are shown in Figure 10a for the models with fixed GW sources for Exp 2, 3 and 4. For most models with fixed GW sources the GW momentum flux entering the stratosphere changes by less than 5% for Exp 3, with the exception of AGCM3-CMAM which shows a 10% decrease of westward momentum flux at 85 hPa, and MRI-ESM2 which shows an 8.8% decrease of eastward momentum flux at 100 hPa. In Exp 4, most momentum flux changes are less than 7.5% relative to Exp 2, except for MRI-ESM2 which shows a 12% increase in eastward momentum flux and 14% increase in westward momentum flux at 100 hPa. MRI-ESM2 has the lowest launching level out of all the models and uses the Hines (1997a,b) schemes, hence the GW spectrum is affected by the increase in N in the lowermost troposphere.

The small change in the tropospheric GW momentum fluxes in Exp 3 and Exp 4 for models with fixed GW sources is due, on average, to the absence of any significant change in zonal winds through which the GW spectrum propagates before entering the stratosphere. For the zonal mean Figure 11a shows that in the tropical troposphere the multi-model mean zonal wind changes by less than 2 m s^{-1} in Exp 3 and 4 relative to Exp 2 and by much less than the differences between the individual models (indicated by the grey lines in the figure showing \pm one inter-model standard deviation). However the zonally averaged zonal wind may not be entirely representative of the local wind profile the GWs propagate through as there are quite significant longitudinal variations in the troposphere (Kawatani et al., 2010). Nonetheless, when averaged, for example, over the western and eastern hemispheres separately (Figures 11b and 11c) there is again little change in tropospheric profiles between Exp 3 and 4 and Exp 2 for the multi-model mean and hence it is reasonable to conclude more generally that in these models there will be little change in GW propagation through the tropical troposphere. Figure 11 shows larger changes in the zonal mean wind, up to 5 m s^{-1} , between Exp 2 and Exp 4 between 120 and 80 hPa. These changes may affect the filtering of GWs in the lowermost part of the QBO, especially for AGCM3-CMAM, which due to its high GW launch level of 90 hPa is very sensitive to the winds in this layer.

Figure 10b shows GW momentum fluxes for models with variable GW sources. The change in 100 hPa GW momentum flux in Exp 3 and Exp 4 relative to Exp 2 is the largest in 60LCAM5 and CESM1(WACCM-110L). In 60LCAM5 and CESM1(WACCM-110L), eastward and westward 100 hPa GW momentum flux averaged between 10°S and 10°N is 20 - 25% larger in Exp 3 than in Exp 2. In Exp 4 these fluxes increase by 48 - 58% (40 - 58%) for eastward (westward) propagating GWs. The changes are very similar when averaged over 5°S to 5°N (not shown). Both 60LCAM5 and CESM1(WACCM-110L) use the Beres (2004) parameterization to calculate GW momentum flux from convectively generated GWs, though with some tuning differences between the two models. In the Beres (2004) parameterization GW momentum flux is proportional to the square of the convective heating rate, which is derived from the convection

parameterization (Richter et al., 2010). Although convective heating is not part of the QBOi output protocol, it is very likely that convective heating increases when convective precipitation increases (this was verified in CESM1(WACCM-110L). In Exp 3 (Exp 4) the precipitation rate averaged over 10°S and 10°N in 60LCAM5 and CESM1(WACCM-110L) increases by 3.5% (5%), which is consistent with the increase in GW momentum flux. Averaged between 10°N and 10°S UMGA7gws shows a change of less than 0.5% in tropical eastward momentum flux in Exp 3 and 4 and a decrease of 4% and 9% in the westward 100 hPa GW momentum flux in Exp 3 and 4 respectively. In UMGA7gws, eastward and westward waves are generated equally and launched at 4 km, with the amplitude of GW momentum flux proportional to the square root of precipitation (Bushell et al., 2015). Averaged over the entire 10°S and 10°N domain, monthly mean precipitation increases by ~ 3% in both Exp 3 and Exp 4 in UMA7gws, however there are regions of both increased and decreased precipitation. The GW momentum flux, dependent on the square root of precipitation, increases in the region of enhanced precipitation over the ITCZ, but decreases in the Indian Ocean and east of Brazil (not shown). The net effect is a slight decrease in GW momentum flux averaged over the 10°S and 10°N domain in Exp 4, which is probably a consequence of the threshold dependence of GW momentum flux on precipitation used by the UMGA7gws source parameterization. LMDz6 also shows a decrease in 100 hPa eastward and westward GW momentum fluxes averaged between 10°S and 10°N of 5% and 10% in Exp 3 and 10% and 18% in Exp 4, respectively. In LMDz6, GW momentum flux is proportional to the square of convective heating (Lott and Guez, 2013), which is estimated from the precipitation (and not taken directly from the convection parameterization). LMDz6 shows a 2% and 5 % increase in mean annual precipitation between 10°S and 10°N in Exp 3 and Exp 4, however instantaneous data is also not available, which would have allowed for a full understanding of the reason for the decrease of GW momentum fluxes while precipitation increases. In summary, models that directly link the GW sources (60LCAM5 and CESM1(WACCM-110L) to (parameterized) convective heating show an increase in the GW momentum flux entering the stratosphere, while the two models (LMDZ6 and UMGA7gws) that use precipitation as a proxy for convective heating show a decrease and this uncertainty significantly affects how the QBO responds to warming climate as demonstrated below.

4.3 | Resolved waves

Resolved waves are likely to change in Exp 3 and Exp 4 due to changes in tropospheric convection and latent heating, as well as changes in the zonal mean wind in the troposphere, although the latter was shown to be rather small (Figure 11). Tropical precipitation (zonal average between 10°S and 10°N) increases by 1 to 7% in the QBOi models between Exp

3 and Exp 2, and by 2 to 13% between Exp 4 and Exp 2 (not shown), suggesting corresponding changes in convection and latent heating and therefore the generation of large scale waves. Figure 12 shows frequency/zonal wavenumber spectra of the vertical components of the EP flux calculated from 6-hourly output averaged between 85 and 70 hPa and between 10°S and 10°N for Exp 2, and the ratio of Exp 3 and Exp 4 to Exp 2. The spectra were computed using the fast Fourier transform using a 72-day window and 12- 402 day overlap, exactly the same methodology as in Holt et al. (2019). In Figure 12 westward propagating (easterly) waves are represented by negative flux and eastward propagating (westerly) waves are represented by positive flux. Some positive flux appears at negative zonal wavenumbers and some negative flux appears at positive zonal wavenumbers as phase speeds are defined relative to the ground and not the background wind. Spectra in Figure 12 are averaged over 10 years of simulation, except for MIROC-AGCM-LL, UMGA7, and UMGA7gws and for which only 4 years of data were available. For the models for which 10 years of data was available, 4-year averages were also made to see if a shorter averaging period changed the spectra, and only very small differences were found. In addition, total easterly and westerly vertical components of EP flux (i.e. the vertical EP flux due to westward and eastward propagating waves, respectively) calculated from 6-hourly data were compared to the provided monthly means and were found to be the same for the sampled periods, and interannual variations were found to be small due to the annually repeating external forcings. Hence it is tacitly assumed that the limited number of years availability of the daily data does not affect any of the conclusions presented in this study. In most models the upward flux due to westward propagating waves with low phase speeds, between 1 and 10 m s⁻¹, increases by a factor of 1.5 to 2 in Exp 3, and by a factor of 2 to 16 in Exp 4. A similar increase in the upward flux due to slow westward propagating waves was found by Kawatani et al. (2011). The slow westward propagating waves contribute directly to driving of the westward phase of the QBO; however, their contribution is smaller than that from the parameterized GWs in most of the QBOi models (Holt et al., 2019; Bushell et al., 2019).

Figure 13 shows that across all the models there is a robust increase in the vertical component of the EP flux for both eastward and westward propagating waves in Exp 3 and Exp 4. For the eastward propagating (westerly) waves the increases range from 6% to 22.5% in Exp 3 and from 20% to 75% in Exp 4, with the multi-model mean increasing by 12% and 29% in Exp 3 and Exp 4, respectively. For the westward propagating (easterly) propagating waves the increases are even larger: from 18% to 62% in Exp 3 and from 52% to 126% in Exp 4, with the multi-model mean now increasing by 38% in Exp 3 and 91% in Exp 4 (Figure 13). Consequently with the warming climate there is a reduction in the ratio of the westerly to easterly vertical component of EP flux in all models except 60LCAM5 and LMDz6. Figure 7 showed that it is the easterly QBO phase at 10 hPa that primarily decreased in amplitude in Exp 3 and Exp 4, however Figure 13

showed that the easterly component of vertical EP flux increases substantially and more than the westerly component of the vertical EP flux. Hence the connection between changes in QBO amplitude and changes in the vertical component of EP flux is not clear.

4.4 | Correlations

In this section we investigate the correlations between the changes in the QBO forcings noted above, and the responses of the QBO amplitude and period to a warming climate. Correlation does not imply causality, however we find these helpful in identifying the possible causes of changes in the QBO characteristics. The top two panels of Figure 14 show that the percentage change in QBO period is positively correlated with the percentage change in the vertical residual velocity, \bar{w}^* , in the lower stratosphere averaged between 100 to 50 hPa. The linear correlation coefficient is 0.44 in Exp 3 and 0.43 in Exp 4 based on the QBO period change derived from the lag correlation method (see Section 3.1). Similar values are found using the TT method and \bar{w}^* at any single level between 100 and 50 hPa. Although not significant these correlations suggest a lengthening of the QBO periods as upwelling increases, as might be expected, but do not fully explain the QBO period response. Instead Figure 14c-f shows that changes in the GW momentum flux entering the stratosphere have a stronger influence on (or at least are better correlated with) the QBO period with correlation coefficient for the eastward and westward GW momentum fluxes, respectively, of -0.63 and -0.82 in Exp 3 and -0.81 and -0.89 in Exp 4. All these correlations are significant at the 95% confidence level apart from the -0.63 in Figure 14c. Hence, larger GW momentum flux entering the stratosphere is most likely the key quantity leading to a shorter QBO period among the QBOi models. In all the panels in the top three rows of Figure 14 there is an evident clustering of models with large changes in GW momentum flux (60LCAM5, CESM1(WACCM-110L), and MRI-ESM2) and those that have small changes in GW momentum flux near 100 hPa. Changes in the easterly and westerly vertical component of the EP flux (bottom two rows of Figure 14) are not as well correlated to changes in QBO period with correlation coefficients of less than 0.1 for westerly component of EP flux, and correlations of -0.56 (-0.34) for the easterly component for Exp 3 (Exp 4) which are found not to be significant. Hence, we conclude that resolved waves do not play a large role in driving the QBO period changes in the QBOi models.

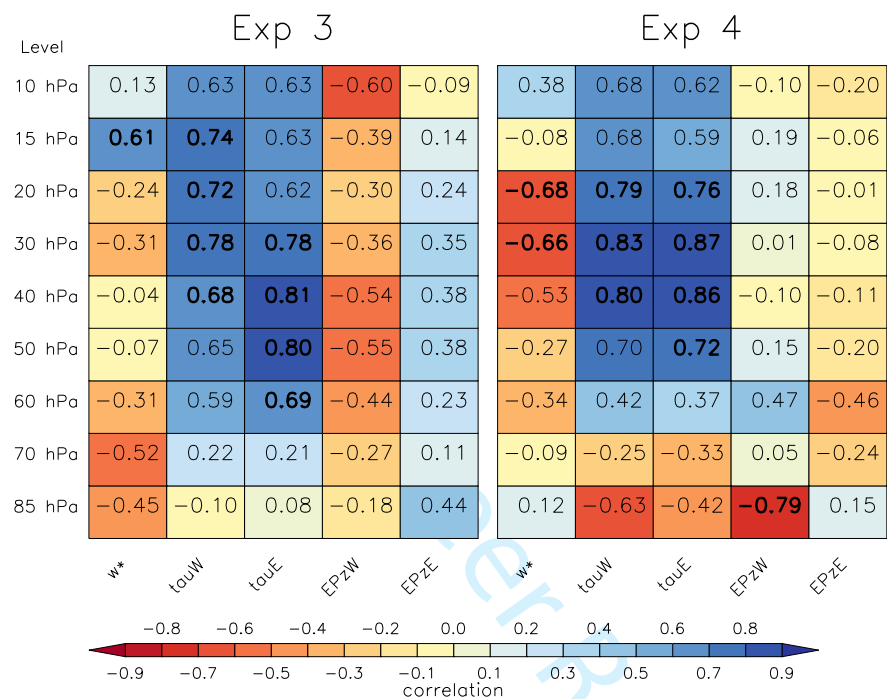
Figure 8 showed that QBO amplitude not only changes with warming climate, but that the relative change varies with altitude and is largest between 60 and 50 hPa. Relative changes in the vertical component of residual velocity also vary with height and are strongest between 80 and 30 hPa (Figure 9b and 9c). Hence, in general, the correlations

between the percentage change in the QBO forcings and percentage change in the QBO amplitude are altitude dependent as can be seen in Table 4 for all levels between 85 and 10 hPa. Levels at which the correlations or anti-correlations are strongest are illustrated in Figure 15. In Exp 3 the QBO amplitude change is correlated with \bar{w}^* above 15 hPa, where the correlation coefficient is largest, and is anti-correlated below with the strongest anti-correlation at 70 hPa, where the increase in \bar{w}^* is maximum (cf. Figure 9b). In Exp 4, consistent with the upward shift to the vertical profile of \bar{w}^* (Figure 9a) the strongest anti-correlation with the amplitude response occurs higher, between 40 and 20 hPa, and is now statistically significant. These anti-correlations in the region of large \bar{w}^* strongly suggest that the increase in tropical upwelling is a significant contributor to the amplitude decrease among the QBOi models.

A strong and significant correlation between the change in GW momentum flux entering the stratosphere and QBO amplitude (Figure 15c-15f), suggests that the QBO amplitude response is also influenced by changes to the parameterized GWs, especially above 50 hPa. In particular, while changes in \bar{w}^* are most likely the main cause of QBO amplitude changes in the lower stratosphere, the changes in GW momentum flux entering the stratosphere appear to be a more significant contributor to the changes in QBO amplitudes at higher levels. This seems consistent with the results of Saravanan (1990) who used a generalization of the original Holton and Lindzen (1972) idealized model of the QBO. In Saravanan's study the vertical advection behaved as a damping, which competed with the tendency of the wave forcing to produce an oscillation. Near the lower boundary this damping effect dominated over the wave forcing, but became weaker at higher altitudes, as found here. However, based on the sign of the correlations in Table 4, neither the increase in \bar{w}^* nor the increase in GW momentum flux entering the stratosphere can simply explain the decrease in the amplitude at 10 hPa in the QBOi models (Figure 8a).

Correlations with westerly component of the vertical EP flux, $F_z W$, (Figure 15g, h) suggest that the QBO amplitude decreases as $F_z W$ increases. The increase in the westerly component of EP flux primarily occurs at very low phase speeds (less than 5 m s^{-1} — see right hand column of Figure 12). It is difficult to interpret exactly how these changes influence QBO amplitude, as the relative roles of resolved and parameterized waves in driving the QBO differ among models (Bushell et al. (2019), Figure 12). Correlations with $F_z W$ and $F_z E$ were also calculated separately for the eastward and westward phases but coefficients were even lower and a robust signal could not be identified. We conclude that resolved waves may play a role in the change of QBO amplitude, however each model's differing momentum budget would need to be considered, which is beyond the scope of this paper.

TABLE 4 Linear correlation coefficient at different pressure levels between % change in QBO amplitude and % change in the vertical residual velocity at that level, w^* , easterly GW momentum flux at 100 hPa, TauE, and westerly gravity wave momentum flux at 100 hPa, TauW, easterly vertical component of EP flux, EpzE, and westerly vertical component of EP flux, EpzW, in Exp 3 and Exp 4 relative to Exp 2. Correlations significant at the 95 % level are bolded. Colors indicate the level of correlation.



5 | DISCUSSION AND CONCLUSIONS

We have presented here potential changes to the QBO in a warming climate based on eleven general circulation models that participated in QBOi Experiments 2, 3, and 4. QBOi Exp 2 is a present day time-slice experiment with annually repeating sea surface temperatures and present day CO₂. In Exp 3 (Exp 4), SSTs were increased by 2 K (4K) and CO₂ was doubled (quadrupled). The changes in external forcings were substantial, especially in Exp 4 compared to present day, largely to elucidate whether convergence in the response among the different models would occur under such scenarios. All of the models that participated in the experiments were able to simulate realistic characteristics of the QBO in present day, as summarized by Bushell et al. (2019). No changes to gravity wave parameterization (or other physical parameterizations, or any other model aspect) were made in the models between Exp 2, 3, and 4.

We found a lack of consistency in the response of the QBO period to a warming climate among the QBOi models.

Three of the models found a substantial decrease in the QBO period, by 5 to 9 months in Exp 3, and by 7 to 14 months in Exp 4. Three of the models found a lengthening of the QBO period by 2 to 13 months in Exp 3, and by 2 to 10 months in Exp 4, while other models exhibited little change (less than 2 months). In a multi-model mean, there is little change in the QBO period in warming climate. In several models in Exp 4 the coherent structure of the QBO characterized by alternating downward propagating easterly and westerly shear zones was lost; however, an oscillation in deseasonalized zonal mean wind was still detected. Vertical residual velocity in the tropical lower stratosphere was found to increase in all QBOi models in Exp 3 and Exp 4, and a positive (although statistically insignificant) correlation between its increase and increase in QBO period was found. We found that the change in QBO period had very large and significant correlations with the momentum flux of gravity waves entering the stratosphere, implying that parameterized gravity waves are the primary driver of QBO period changes. Two of the models that predict substantial QBO period shortening in Exp 3 and Exp 4, 60LCAM5 and CESM1(WACCM5-110L), include a parameterization of gravity wave sources based on Beres et al. (2004), which predicts that in a warming climate eastward (westward) momentum flux at 100 hPa would increase by ~25% (20%) in Exp 3 and ~53% (44%) in Exp 4. MRI-ESM2, the third model predicting shortening of the QBO period showed a ~8% (20%) increase in source level gravity wave flux in Exp 3 (Exp 4) due to GW launching at the surface and increased buoyancy frequency at that level. We found no relation between changes in QBO period and change in the vertical component of the EP flux, however the driving from resolved waves is smaller than that from parameterized waves in the QBOi models, except for in MIROC-AGCM-LL (Bushell et al., 2019; Holt et al., 2019).

Unlike changes in the QBO period, the Exp 3 and Exp 4 simulations showed a robust response across the QBOi models in terms of QBO amplitude changes. All of the models project a decrease of the QBO amplitude in the warming climate. The projected QBO amplitude decrease varies with height and is strongest near 60 hPa, reaching a decrease of 36% in Exp 3 and 51% in Exp 4 at that level. The QBO amplitude reduction at 10 hPa occurred primarily in the easterly phase in all QBOi models. The QBO amplitude decrease in the lower tropical stratosphere is correlated with an increase in vertical residual velocity in that region. The residual vertical velocity increases by 50% in Exp 3 and by 100% in Exp 4 in a multi-model mean between 60 and 80 hPa. The decrease of QBO amplitude with warming climate, and relation to changes in tropical upwelling, is consistent with findings of Kawatani and Hamilton (2013) who found observational evidence in QBO amplitude weakening. From about 60 hPa upward, the QBO amplitude change is positively correlated with the change in gravity wave momentum flux entering the stratosphere, such that smaller amplitude reductions occur in models that have increased GW flux. These relations are consistent with the findings of Saravanan (1990), who used a generalization of the original Holton and Lindzen (1972) idealized QBO model to show that the QBO amplitude

1
2 471 at its lowest altitudes is damped by upwelling at those altitudes. However, it is also possible that the reasons for the
3
4 472 amplitude decrease differ between the models. In this study we also found a negative correlation between the westerly
5 473 component of the vertical EP flux and change in QBO amplitude in Exp 3; however, due to differing relative roles of
6
7 474 resolved waves and parametrized waves in driving the QBO among models these changes seemed less robust and more
8 475 difficult to interpret.

10
11
12 476 The largest uncertainty in the response of the QBO in warming climate comes from the representation of pa-
13
14 477 rameterized gravity waves in climate models. This was clear from this study utilizing eleven different GCMs, and is
15
16 478 consistent with the study of Schirber et al. (2015) who conducted sensitivity tests using a single GCM with four different
17 479 gravity wave parameterization configurations. Most GCMs at this time still use GW parameterization with gravity
18
19 480 wave sources that are fixed and don't change with changes in tropospheric climate. This assumption is likely to be
20 481 erroneous, and hence four of the models that participated in this study have employed a source-based gravity wave
21
22 482 parameterization. However, as was shown in Figure 10b, different GW source parameterizations predict different
23
24 483 changes to GW momentum flux spectra entering the stratosphere, creating more uncertainty rather than convergence
25 484 with regard to how gravity waves are likely to change in the future climate. A better understanding of how gravity wave
26
27 485 sources will change in the future climate is crucial to improving projections of how the QBO will change in the future.
28 486 MIROC-AGCM-LL, the only model in this study without a gravity wave parameterization, predicts a QBO amplitude
29
30 487 decrease in a warming climate similarly to all the other QBOi models in Exp 4 (but predicts no change for Exp 3), and
31
32 488 predicts a slight QBO period increase in a warming climate, similarly to some models with fixed and similarly to some
33 489 models with variable gravity wave sources. That response is also uncertain as the resolved wave spectra, primarily
34
35 490 Kelvin and mixed-Rossby GWs in MIROC-AGCM-LL differ from observations in several aspects (Holt et al., 2019). Most
36
37 491 GCMs still under-resolve the forcing due to Kelvin and mixed-Rossby GWs (Holt et al., 2019) and hence the forcing of
38 492 the QBO is strongly dependent on gravity wave parameterizations. The inadequate representation of large scale waves
39
40 493 also brings into question the confidence in the response of these waves to a warming climate. Our study has shown that
41 494 the westerly and especially the easterly vertical component of the EP flux are likely to increase in a warmer climate,
42
43 495 however these estimates are dependent on changes in tropical precipitation in GCMs which carry biases even in present
44
45 496 day climate. Hence, although this study has made significant progress in quantifying QBO changes in warming climate
46 497 by utilizing multiple models, and is the first to do so, much uncertainty needs to be resolved before confidence in the
47
48 498 response of the QBO changes is reached.

ACKNOWLEDGEMENTS

We acknowledge the scientific guidance of the WCRP for helping motivate this work, coordinated under the framework of the Stratosphere-troposphere Processes and their Role in Climate (SPARC) QBO initiative (QBOi) led by JA, NB, KH and SO. The QBOi data archive was kindly hosted by the Centre for Environmental Data Analysis (CEDA). This material is based upon work supported by the National Center for Atmospheric Research, which is a major facility sponsored by the National Science Foundation under Cooperative Agreement No. 1852977. NB was supported by the Met Office Hadley Centre Programme funded by BEIS and Defra, and by the European Commission's Seventh Framework Programme StratoClim project 226520. YK was supported by Japan Society for Promotion of Science (JSPS) KAKENHI Grant Numbers JP15KK0178, JP17K18816 and JP18H01286. YK and KH were supported by the Japan Agency for Marine-Earth Science and Technology (JAMSTEC) through its sponsorship of research at the International Pacific Research Center. SW and YK were partly supported by a Japan Science and Technology Agency (JST) as part of the Belmont Forum GOTHAM project, and by the "Integrated Research Program for Advancing Climate Models (TOUGOU program)" from the Ministry of Education, Culture, Sports, Science and Technology (MEXT), Japan. FL, SW, YK, LG and SO acknowledge funding for the Belmont Forum JPI-Climate GOTHAM project from: Agence Nationale Recherche (ANR-15-JCLI-0004-01), the Japan Science and Technology Agency and the Natural Environment Research Council (NE/P006779/1 and NE/M005828/1). LG and SO are supported by the UK Natural Environment Research Council (NERC) through the National Centre for Atmospheric Science (NCAS). The Earth Simulator was used for MIROC-ESM and MIROC-AGCM-LL simulations. For the EMAC simulations, PB, TK, and SV acknowledge support by the state of Baden-Württemberg through bwHPC. CC and FS have been supported by the Copernicus Climate Change Service, funded by the EU and implemented by ECMWF. We thank Elisa Manzini for helpful comments in the early stages of the manuscript.

REFERENCES

- Andrews, D. G., Holton, J. R. and Leovy, C. B. (1987) *Middle Atmosphere Dynamics*. Academic Press.
- Arakawa, A. and Schubert, W. H. (1974) Interactions of cumulus cloud ensemble with the large-scale environment. *J. Atmos. Sci.*, **31**, 674–701.
- Austin, J., Shindell, D., Beagley, S. R., Dameris, M., Manzini, E., Nagashima, T., Newman, P. A., Pitari, G., Rozanov, E., Schnadt, C.

1
2 525 and Shepherd, T. G. (2003) Uncertainties and assessments of chemistry-climate models of the stratosphere. *Atmospheric*
3 526 *Chemistry and Physics*, **3**, 1–27.

4
5 527 Baldwin, M. P., Gray, L., Dunkerton, T. J., Hamilton, K., Haynes, P. H., Randel, W. J., Holton, J. R., Alexander, M., Hirota, I., Hori-
6 528 nouchi, T., Jones, D. B. A., Kinnnersley, J. S., Marquardt, C., Sato, K. and Takahashi, M. (2001) The Quasi-Biennial Oscillation.
7 529 *Review of Geophysics*, **39**, 179–229.

8
9
10 530 Barnes, E. A. and Polvani, L. (2013) Response of the midlatitude jets, and of their variability, to increased greenhouse gases in
11 531 the CMIP5 models. *Journal of Climate*, **26**, 7117–7135.

12
13 532 Beres, J. H. (2004) Gravity Wave Generation by a Three-Dimensional Thermal Forcing. *J. Atmos. Sci.*, **61**, 1805–1815.

14
15 533 Beres, J. H., Alexander, M. J. and Holton, J. R. (2004) A method of specifying the gravity wave spectrum above convection based
16 534 on latent heating properties and background wind. *J. Atmos. Sci.*, **61**, 324–337.

17
18 535 Bushell, A., Anstey, J., Butchart, N., Kawatani, Y., Osprey, S., Richter, J., Serva, F., Braesicke, P., Cagnazzo, C., Chen, C.-C., Chun, H.-
19 536 Y., Garcia, R., Gray, L. J., Hamilton, K., Kerzenmacher, T., Kim, Y.-H., Lott, F., McLandress, C., Naoe, H., Scinocca, J., Stockdale,
20 537 T. N., Watanabe, S., Yoshida, K. and Yukimoto, S. (2019) The Quasi-Biennial Oscillation in global climate models: present-
21 538 day conditions. *Quarterly Journal of the Royal Meteorological Society*, In preparation.

22
23
24 539 Bushell, A. C., Butchart, N., Derbyshire, S. H., Jackson, D. R., Shutts, G. J., Vosper, S. B. and Webster, S. (2015) Parameterized
25 540 Gravity Wave Momentum Fluxes from Sources Related to Convection and Large-Scale Precipitation Processes in a Global
26 541 Atmosphere Model. *Journal of the Atmospheric Sciences*, **72**, 4349–4371.

27
28
29 542 Butchart, N., Anstey, J., Hamilton, K., Osprey, S., McLandress, C., Bushell, A., Kawatani, Y., Kim, Y.-H., Lott, F., Scinocca, J., Stock-
30 543 dale, T., Andrews, M., Bellprat, O., Braesicke, P., Cagnazzo, C., Chen, C.-C., Chun, H.-Y., Dobrynin, M., Garcia, R., Garcia-
31 544 Serrano, J., Gray, L., Holt, L., Kerzenmacher, T., Naoe, H., Pohlmann, H., Richter, J., Scaife, A., Schenzinger, V., Serva, F.,
32 545 Versick, S., Watanabe, S., Yoshida, K. and Yukimoto, S. (2018) Overview of experiment design and comparison of models
33 546 participating in phase 1 of the SPARC Quasi-Biennial Oscillation initiative (QBOi). *Geoscientific Model Development*, **11**,
34 547 1009–1032.

35
36
37
38 548 Butchart, N., Cionni, I., Eyring, V., Shepherd, T. G., Waugh, D. W., Akiyoshi, H., Austin, J., Brühl, C., Chipperfield, M. P., Cordero, E.,
39 549 Dameris, M., Deckert, R., Dhomse, S., Frith, S. M., Garcia, R. R., Gettelman, A., Giorgetta, M. A., Kinnison, D. E., Li, F., Mancini,
40 550 E., McLandress, C., Pawson, S., Pitari, G., Plummer, D. A., Rozanov, E., Sassi, F., Scinocca, J. F., Shibata, K., Steil, B. and Tian, W.
41 551 (2010) Chemistry-climate model simulations of twenty-first century stratospheric climate and circulation changes. *Journal*
42 552 *of Climate*, **23**, 5349–5374.

43
44
45 553 Butchart, N., Scaife, A. A., Bourqui, M., Grandpré, J., Hare, S. H., Kettleborough, J., Langematz, U., Manzini, E., Sassi, F., Shi-
46 554 bata, K., Shindell, D. and Sigmond, M. (2006) Simulations of anthropogenic change in the strength of the Brewer-Dobson
47 555 circulation. *Climate Dynamics*, **27**, 727–741.

48
49
50
51
52
53
54
55

- Dee, D. P., Uppala, S. M., Simmons, A. J., Berrisford, P., Poli, P., Kobayashi, S., Andrae, U., Balmaseda, M. A., Balsamo, G., Bauer, P., Bechtold, P., Beljaars, A. C. M., van de Berg, L., Bidlot, J., Bormann, N., Delsol, C., Dragani, R., Fuentes, M., Geer, A. J., Haimberger, L., Healy, S. B., Hersbach, H., V., H. E., Isaksen, I., Kallberg, P. W., Kohler, M., Matricardi, M., McNally, A. P., Monge-Sanz, B. M., Morcrette, J.-J., Park, B. K., Peubey, C., P., d. R., Tavolato, C., Thepaut, J. N. and Vitart, F. (2011) The ERA-Interim reanalysis: Configuration and performance of the data assimilation system. *Quarterly Journal of the Royal Meteorological Society*, **656**, 553–597.
- Dunkerton, T. J. (1991) Nonlinear propagation of zonal winds in an atmosphere with Newtonian cooling and equatorial wavelike driving. *J. Atmos. Sci.*, **48**, 236–263.
- Dunkerton, T. J. and Delisi, D. P. (1985) Climatology of the Equatorial Lower Stratosphere. *Journal of the Atmospheric Sciences*, **42**, 376–396.
- Fu, Q., Solomon, S. and Hartmann, D. L. (2015) Observational evidence of strengthening of the Brewer–Dobson circulation since 1980. *J. Geophys. Res.*, **120**, 10214–10228.
- Garcia, R. R. and Randel, W. J. (2008) Acceleration of the Brewer – Dobson Circulation due to Increases in Greenhouse Gases. *Journal of the Atmospheric Sciences*, **65**, 2731–2739.
- Giorgetta, M. A. and Doege, M. C. (2005) Sensitivity of the quasi-biennial oscillation to CO₂ doubling. *Geophys. Res. Lett.*, **32**, 2–5.
- Hines, C. O. (1997a) Doppler-spread parametrization of gravity-wave momentum deposition in the middle atmosphere. Part 1: Basic formulation. *Journal of Atmospheric and Solar-Terrestrial Physics*, **59**, 371–386.
- (1997b) Doppler-spread parametrization of gravity-wave momentum deposition in the middle atmosphere. Part 2: Broad and quasi monochromatic spectra, and implementation. *Journal of Atmospheric and Solar-Terrestrial Physics*, **59**, 387–400.
- Holt, L., Lott, F., Garcia, R., Kiladis, G. N., Anstey, J., Braesicke, P., Bushell, A., Butchart, N., Cagnazzo, C., Chen, C.-C., Chun, H.-Y., Hamilton, K., Kawatani, Y., Kerzenmacher, T., Kim, Y.-H., McLandress, C., Naoe, H., Osprey, S., Richter, J., Scinocca, J., Serva, F., Versick, S., Watanabe, S., Yoshida, K. and Yukimoto, S. (2019) An evaluation of tropical waves and wave forcing of the QBO in the QBOi models. *Quart. J. Roy. Meteor. Soc.*, In preparation.
- Holton, J. R. and Lindzen, R. S. (1972) An updated theory for the quasi-biennial cycle of the tropical stratosphere. *J. Atmos. Sci.*, **29**, 1076–1080.
- Kawatani, Y. and Hamilton, K. (2013) Weakened stratospheric quasibiennial oscillation driven by increased tropical mean upwelling. *Nature*, **497**, 478–481.
- Kawatani, Y., Hamilton, K. and Watanabe, S. (2011) The Quasi-Biennial Oscillation in a Double CO₂ Climate. *Journal of the Atmospheric Sciences*, **68**, 265–283.

26

J.H. RICHTER ET AL.

1

2 586 Kawatani, Y., Watanabe, S., Sato, K., Dunkerton, T. J., Miyahara, S. and Takahashi, M. (2010) The Roles of Equatorial Trapped

3 587 Waves and Internal Inertia–Gravity Waves in Driving the Quasi-Biennial Oscillation. Part II: Three-Dimensional Distribu-

4 588 tion of Wave Forcing. *Journal of the Atmospheric Sciences*, **67**, 981–997.

5

6 589 Lin, P. and Waugh, D. W. (2013) Changes in various branches of the Brewer–Dobson circulation from an ensemble of chemistry

7 590 climate models. *J. Geophys. Res.*, **117**, D20119, doi:10.1029/2012JD017905.

8

9

10 591 Lindzen, R. S. (1981) Turbulence and Stress Owing to Gravity Wave and Tidal Breakdown. *J. Geophys. Res.*, **86**, 9707–9714.

11

12 592 Lott, F. and Guez, L. (2013) A stochastic parameterization of the gravity waves due to convection and its impact on the equato-

13 593 rial stratosphere. *Journal of Geophysical Research Atmospheres*, **118**, 8897–8909.

14

15 594 Lott, F., Guez, L. and Maury, P. (2012) A stochastic parameterization of non-orographic gravity waves, Formalism and impact

16 595 on the equatorial stratosphere. *Geophys. Res. Lett.*, **39**, doi:10.1029/2012GL051001.

17

18 596 McLandress, C. and Shepherd, T. G. (2009) Impact of climate change on stratospheric sudden warmings as simulated by the

19 597 Canadian Middle Atmosphere model. *Journal of Climate*, **22**, 5449–5463.

20

21

22 598 Naujokat, B. (1986) An update to the observed quasi-biennial oscillation of stratospheric winds over the tropics. *J. Atmos. Sci.*,

23 599 **43**, 1873–1877.

24

25 600 Richter, J. H., Sassi, F. and Garcia, R. R. (2010) Towards a physically based gravity wave source parameterization in a general

26 601 circulation model. *J. Atmos. Sci.*, **67**, 136–156.

27

28 602 Saravanan, R. (1990) A multiwave model of the quasi-biennial oscillation. *J. Atmos. Sci.*, **47**, 2465–2474.

29

30 603 Schirber, S., Manzini, E., Krismer, T. and Giorgetta, M. (2015) The quasi-biennial oscillation in a warmer climate: sensitivity to

31 604 different gravity wave parameterizations. *Climate Dynamics*, **45**, 825–836.

32

33

34 605 Shepherd, T. G. and McLandress, C. (2011) A Robust Mechanism for Strengthening of the Brewer–Dobson Circulation in Re-

35 606 sponse to Climate Change: Critical-Layer Control of Subtropical Wave Breaking. *Journal of the Atmospheric Sciences*, **68**,

36 607 784–797. URL: <http://journals.ametsoc.org/doi/abs/10.1175/2010JAS3608.1>.

37

38 608 Simpson, I. R., Shaw, T. A. and Seager, R. (2014) A Diagnosis of the Seasonally and Longitudinally Varying Midlatitude Circula-

39 609 tion Response to Global Warming*. *Journal of the Atmospheric Sciences*, **71**, 2489–2515. URL: <http://journals.ametsoc.org/doi/abs/10.1175/JAS-D-13-0325.1>.

40 610

41

42

43 611 Warner, C. D. and McIntyre, M. E. (1999) Toward an ultra simple spectral gravity wave parameterization for general circulation

44 612 models. *Earth Planets Space*, **51**, 475–484.

45

46 613 Watanabe, S. and Kawatani, Y. (2012) Sensitivity of the QBO to mean tropical upwelling under a changing climate simulated

47 614 with an Earth System Model. *Journal of the Meteorological Society of Japan, Series II*, **90A**, 351–360.

48

49

50

51

52

53

54

55

Winter, B. and Bourqui, M. (2010) Wave forcing in the stratosphere under doubled-CO₂ conditions in a 100-year coupled chemistry-climate model study. *Journal of Geophysical Research Atmospheres*, **115**, 1–17.

For Peer Review

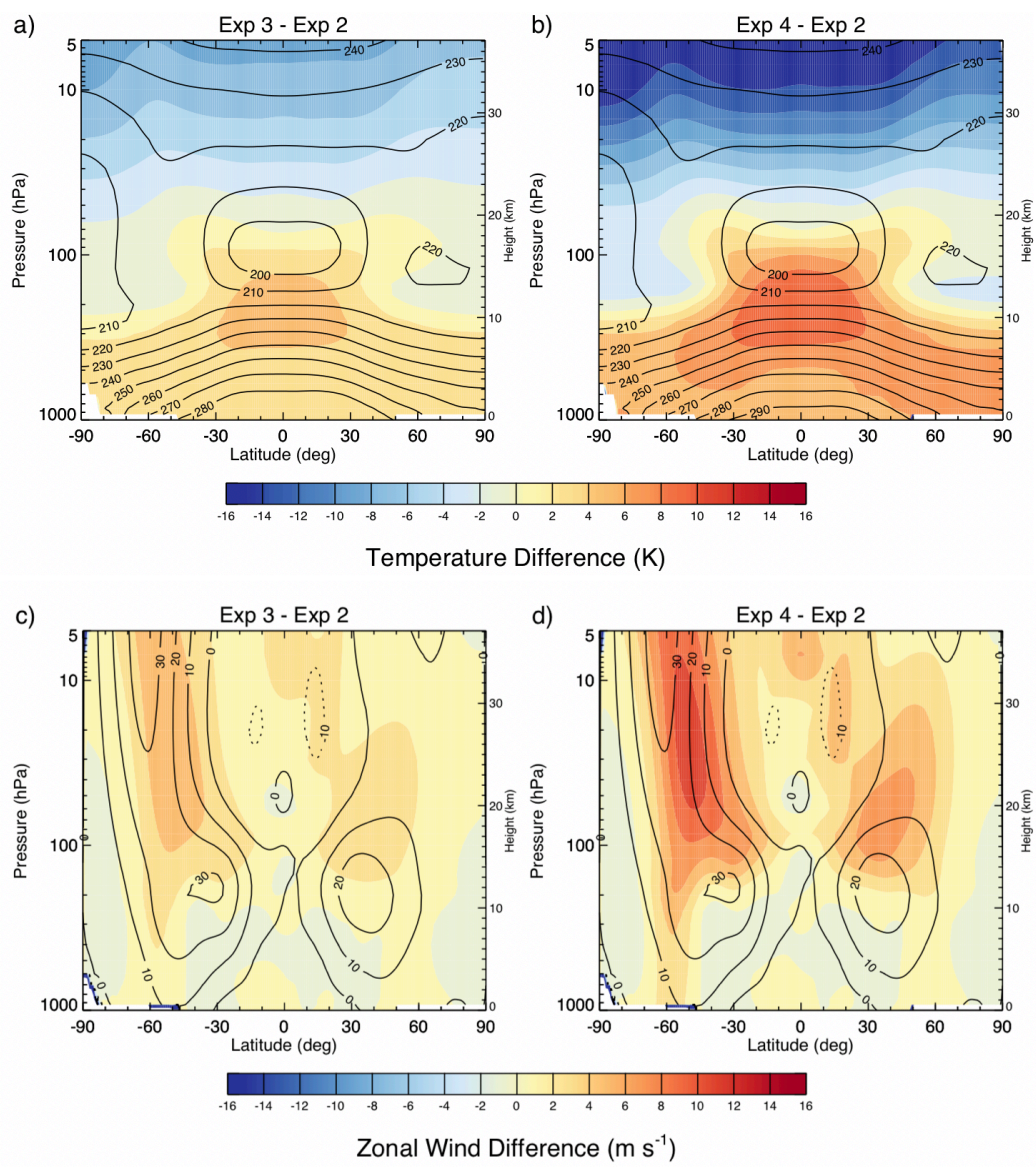


FIGURE 1 Multi-model mean of the change in zonal mean temperature in K (top panel) and zonal mean zonal wind in m s^{-1} (bottom panels) between Exp 3 (left panels) and Exp 4 (right panels) relative to Exp 2. Shading indicates temperature (zonal wind) change and solid contours indicate the multi-model mean for temperature (zonal mean wind) Exp 2 in top (bottom) panels.

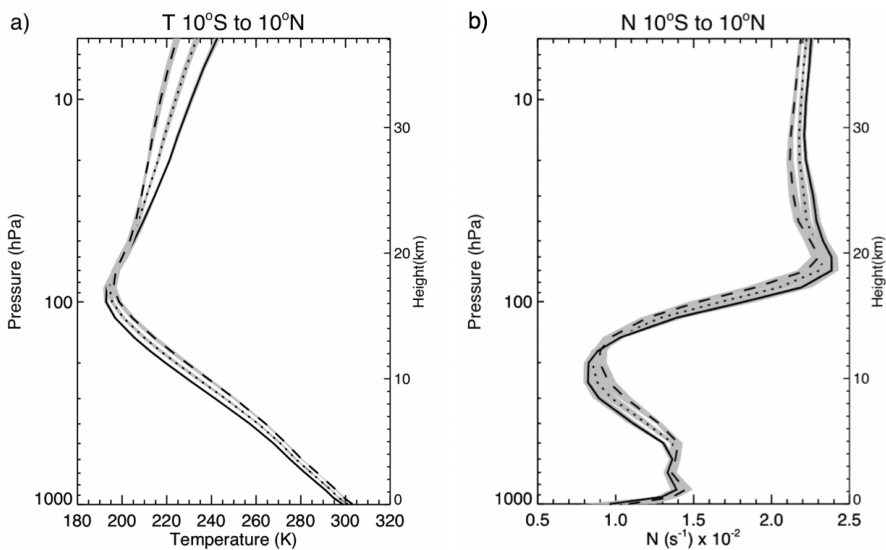


FIGURE 2 Zonal mean temperature (left) and buoyancy frequency (right) averaged between 10°S and 10°S for Exp 2 (solid), Exp 3 (dotted), and Exp 4 (dashed). Grey shading around each line depicts \pm two standard error (2 times the multi-model standard deviation divided by \sqrt{n} , where n is the number of models).

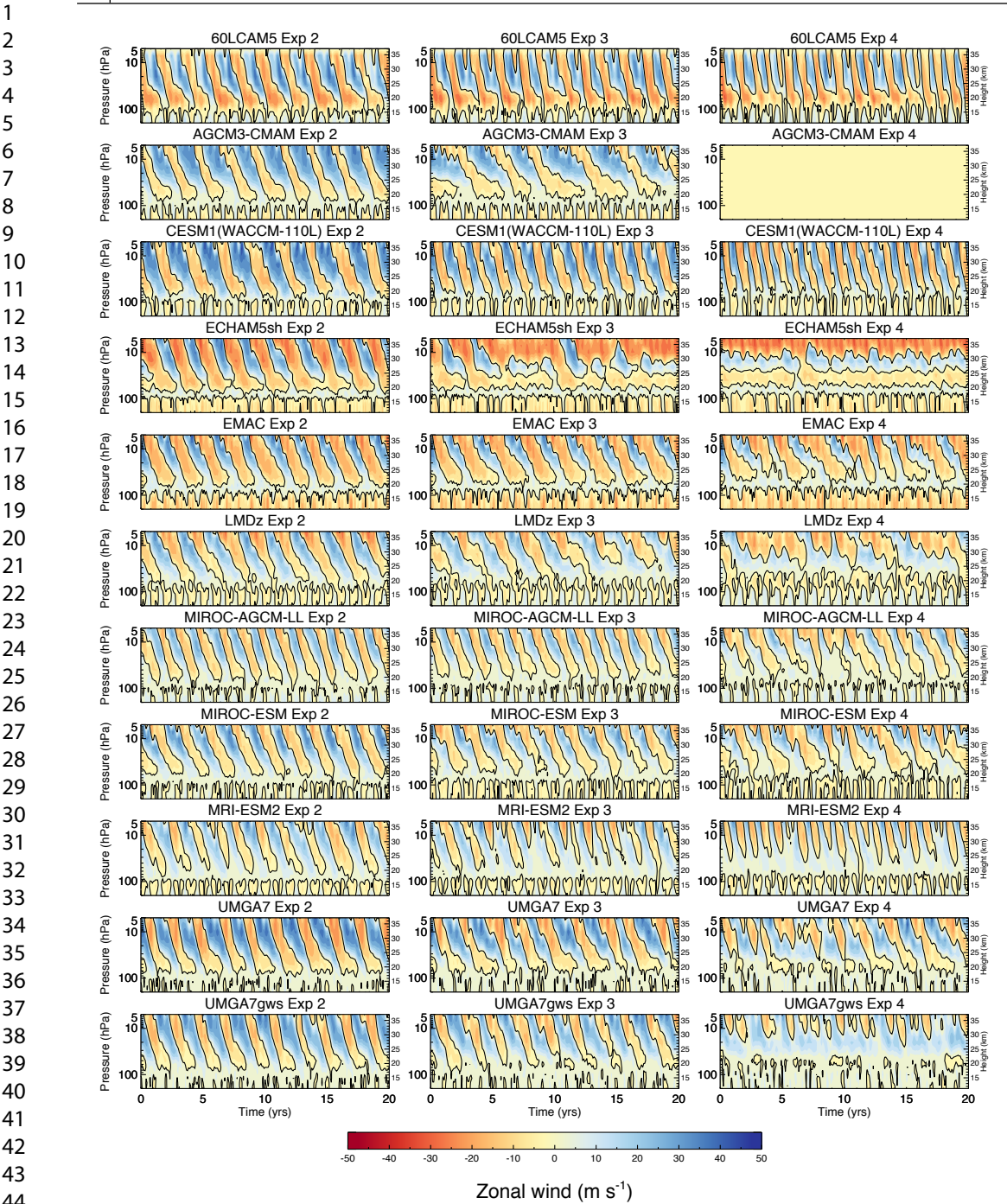


FIGURE 3 Zonal mean zonal wind averaged between 5°S and 5°N as a function of pressure and time for Exp 2 (left column), Exp 3 (middle column) and Exp 4 (right column). First 20 years of the first ensemble for each model is shown. Model names are noted in the panel titles.

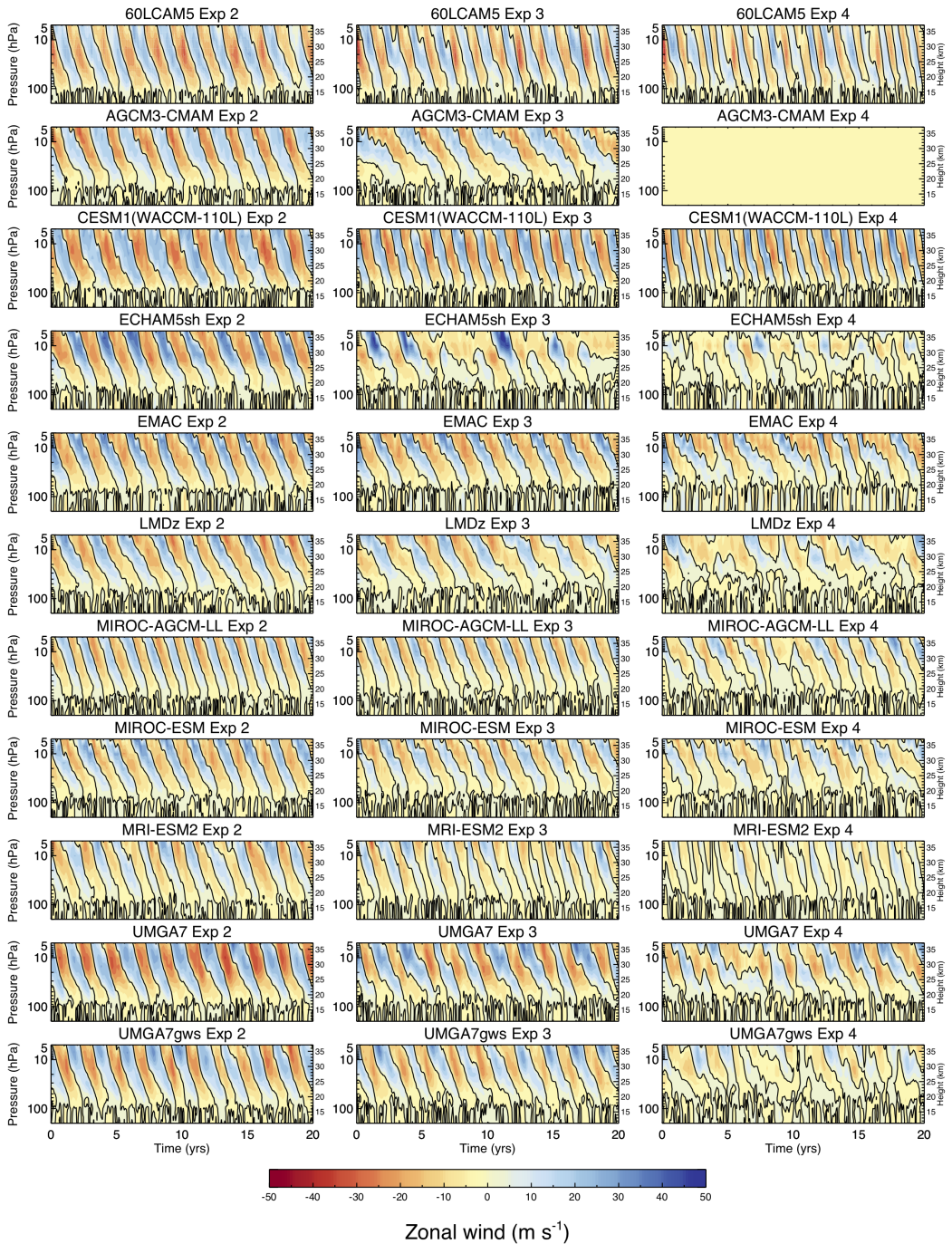


FIGURE 4 Same as Figure 4 but after removing the seasonal cycle.

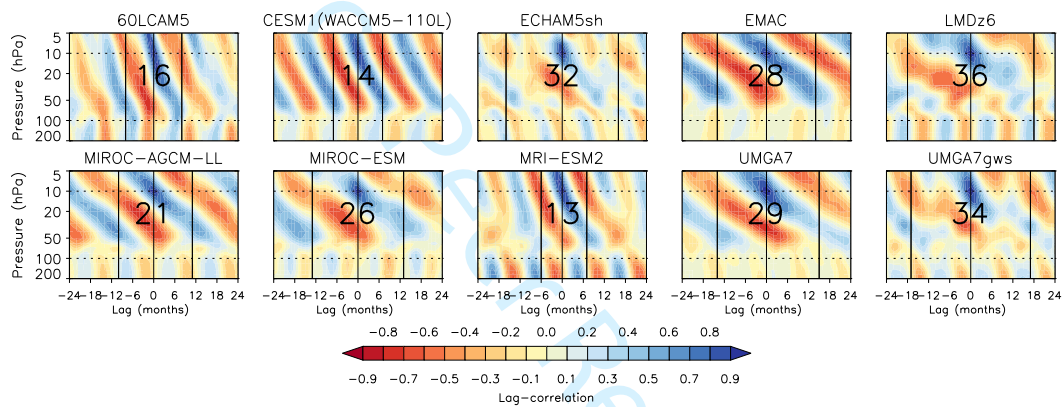


FIGURE 5 Correlation of monthly mean zonal mean eastward wind, \bar{u} , for Exp 4 at a lag as a function of height, $\bar{u}(z, t \pm lag)$ with \bar{u} at 10 hPa, $\bar{u}(z = 10hPa, t)$. The black vertical lines are at $lag = 0$ and at the local minimum correlation (maximum anti-correlation) at 10 hPa either side of the $lag = 0$ line. The large numbers in black denote the number of months between these two lines, interpreted as the period of the oscillating signal seen in the figure.

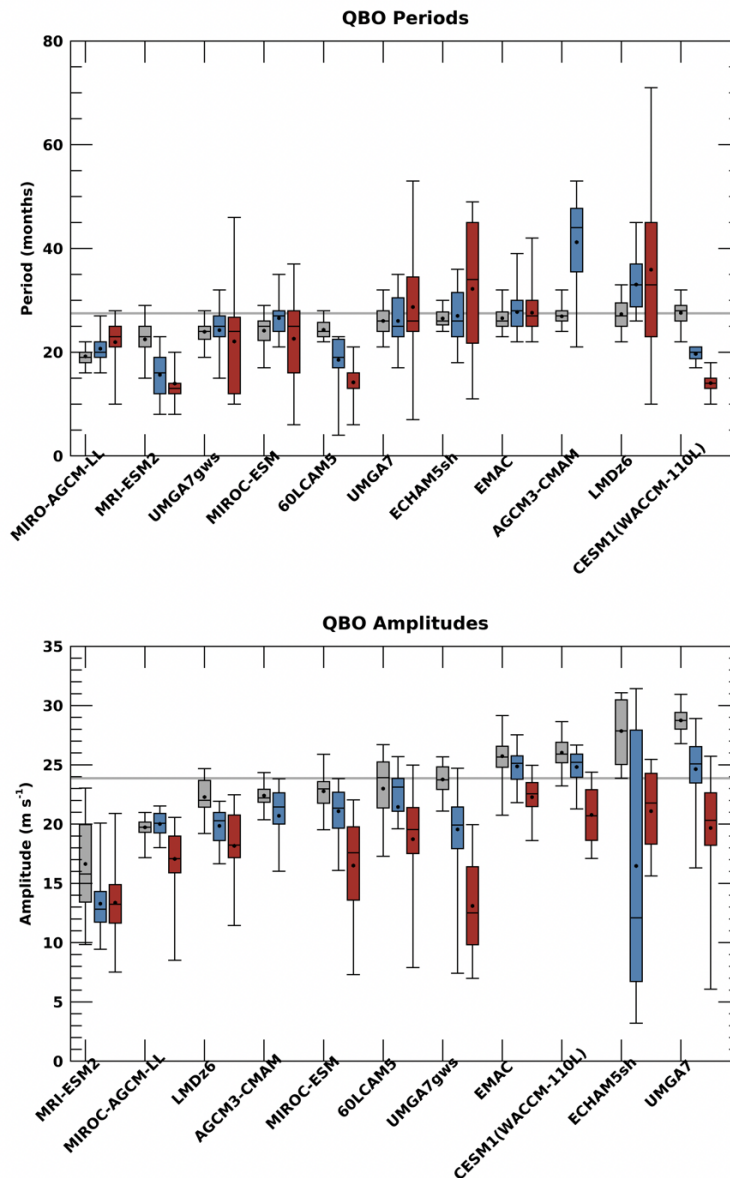


FIGURE 6 Distribution of QBO periods (top) and amplitudes (bottom) in Exp 2 (grey), Exp 3 (blue), and Exp 4 (red) derived using the TT method at 10 hPa. The distribution median is depicted by horizontal line in each box, box edges mark the lower quartile and upper quartiles, box whiskers mark the minimum and maximum values. Black dots represent mean values. Models are ordered according to Exp 2 mean period (top panel) amplitude (bottom panel). Horizontal grey lines indicate present day ERA-Interim reanalysis (Dee et al., 2011) values.

1
2
3
4
5
6
7
8
9
10
11
12
13
14
15
16
17
18
19
20
21
22
23
24
25
26
27
28
29
30
31
32
33
34
35
36
37
38
39
40
41
42
43
44
45
46
47
48
49
50
51
52
53
54
55

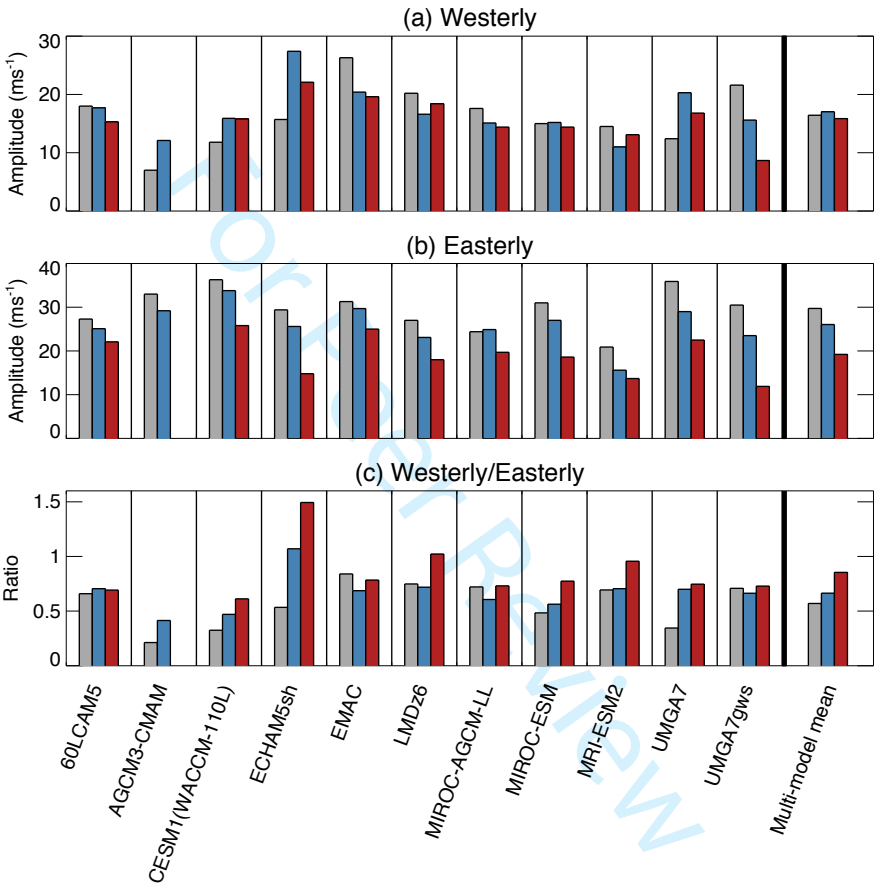


FIGURE 7 QBO amplitude changes at 10 hPa separated by phase derived using the TT method for Exp 2 (gray), Exp 3 (blue) and Exp 4 (red).

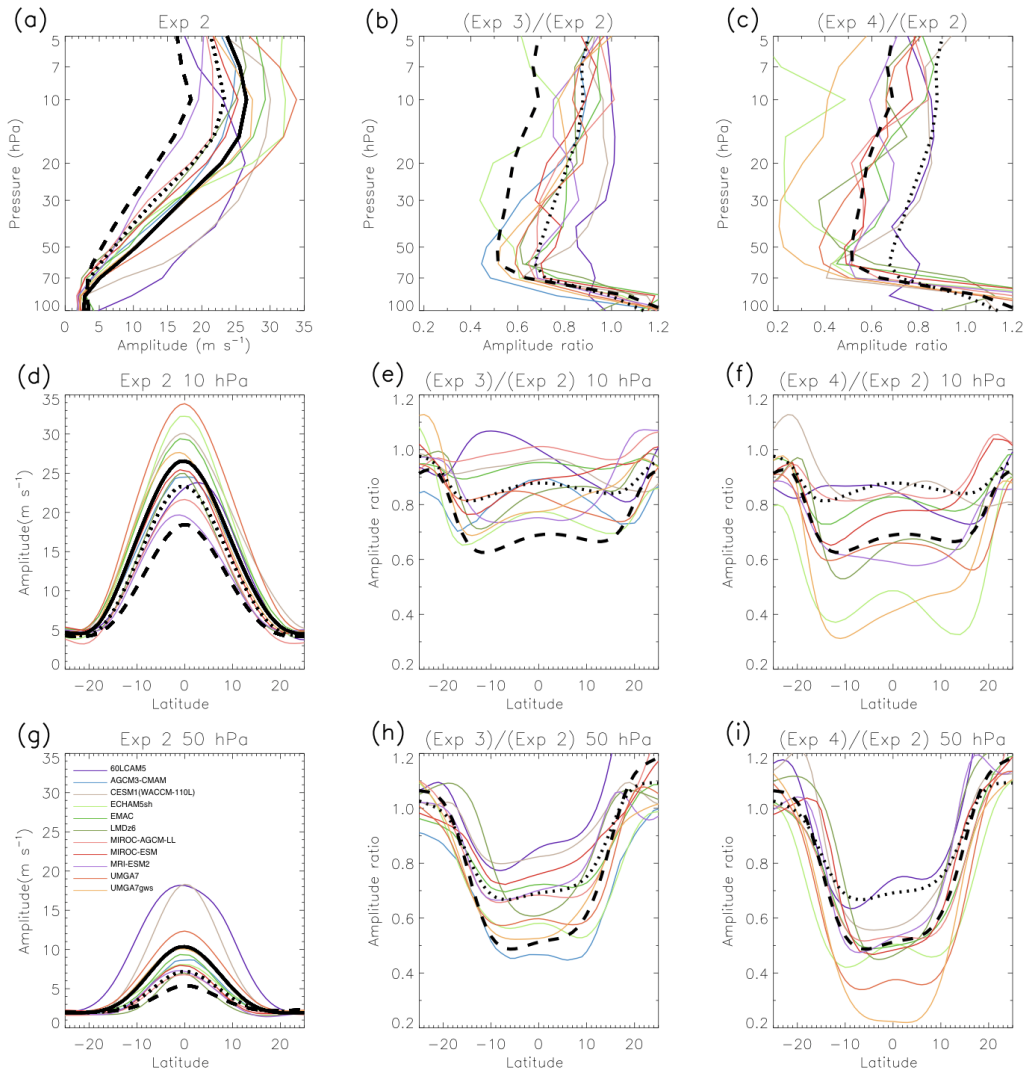


FIGURE 8 Multi-model mean of QBO amplitude calculated using the DD method in m s^{-1} as a function of pressure (top row) and as a function of latitude at 10 hPa (middle row) and 50 hPa (bottom row). In the left column, thin colored lines depict individual model QBO amplitudes for Exp 2 and multi-model means are shown for Exp 2 (thick black solid line), Exp 3 (dotted line), and Exp 4 (dashed line). Middle and right columns depict ratios of QBO amplitudes for Exp 3 to Exp 2 and Exp 4 to Exp 2 respectively, with colored lines depicting individual models and the dotted (dashed) line depicting the multi-model mean of ratios for Exp 3 to Exp 2 (Exp 4 to Exp 2).

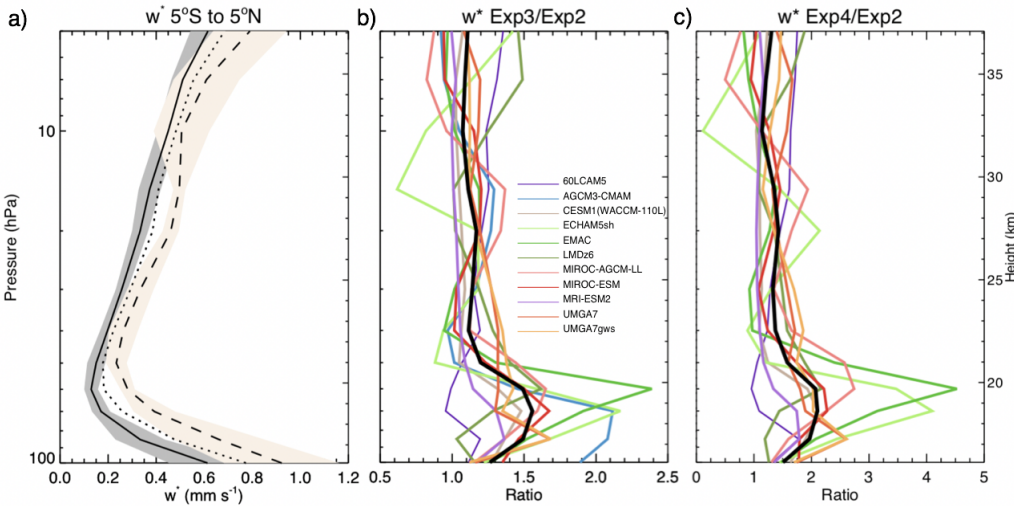


FIGURE 9 Multi-model mean of zonally averaged residual vertical velocity between 5°S to 5°N for Exp 2, 3 and 4 (left panel), and its change from Exp 3 to Exp 2 (center panel) and change from Exp 4 to Exp 2 (right panel). In the left panel solid line represents Exp 2, dotted Exp 3, and dashed Exp 4. Grey (peach) shading around the solid (dashed) line depicts +/- two standard error. In the two rightmost panels, thin coloured lines represent individual models, thick black line is the multi-model mean.

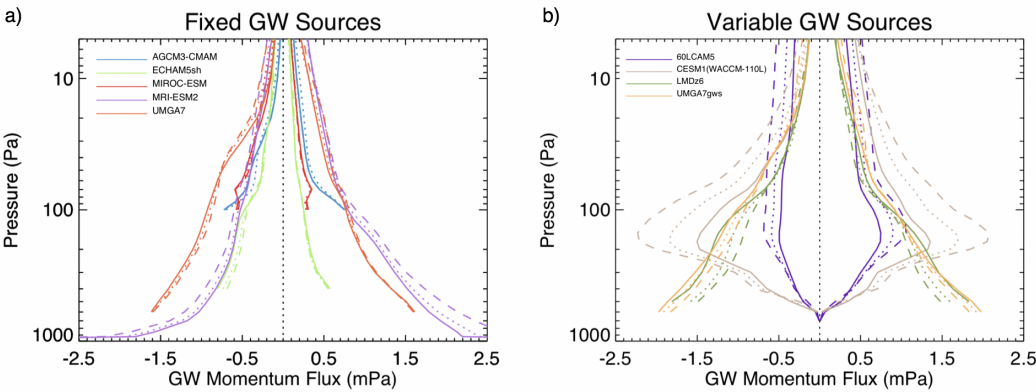


FIGURE 10 Vertical profiles of GW momentum flux averaged between 10°S and 10°N for models with fixed GW source parameterizations (left) and interactive GW sources (right). Solid lines represent Exp 2, dotted lines represent Exp 3 and dashed lines are for Exp 4. Eastward (westward) momentum flux is depicted by positive (negative) values respectively. Note that momentum flux was divided by a factor of 10 for 60LCAM5. GW momentum fluxes were not available for EMAC, and MIROC-AGCM-LL does not use a GW parameterization, hence only nine models are shown.

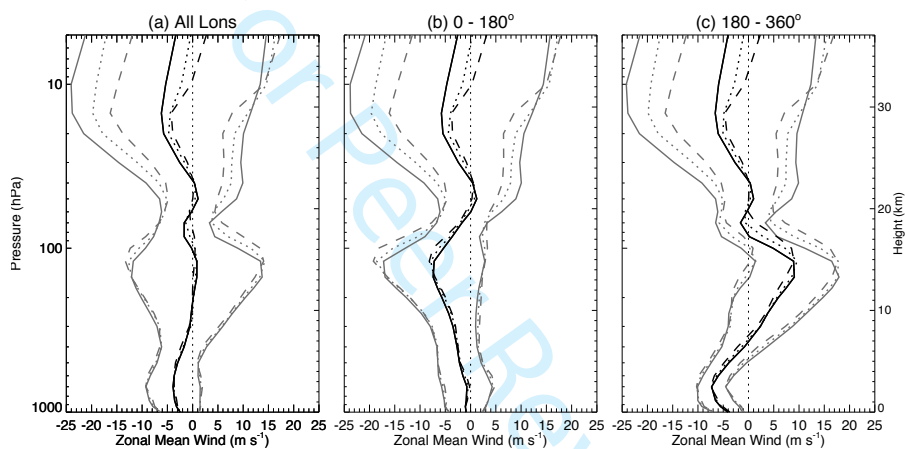


FIGURE 11 Multi-model mean of zonal mean wind averaged between 5°S and 5°N and all longitudes (left), 0 - 180° (middle), and 180 - 360° (right) (Black lines) and multi-model mean \pm one inter-model standard deviation (grey lines). Solid lines are for Exp 2, dotted for Exp 3, and dashed for Exp 4.

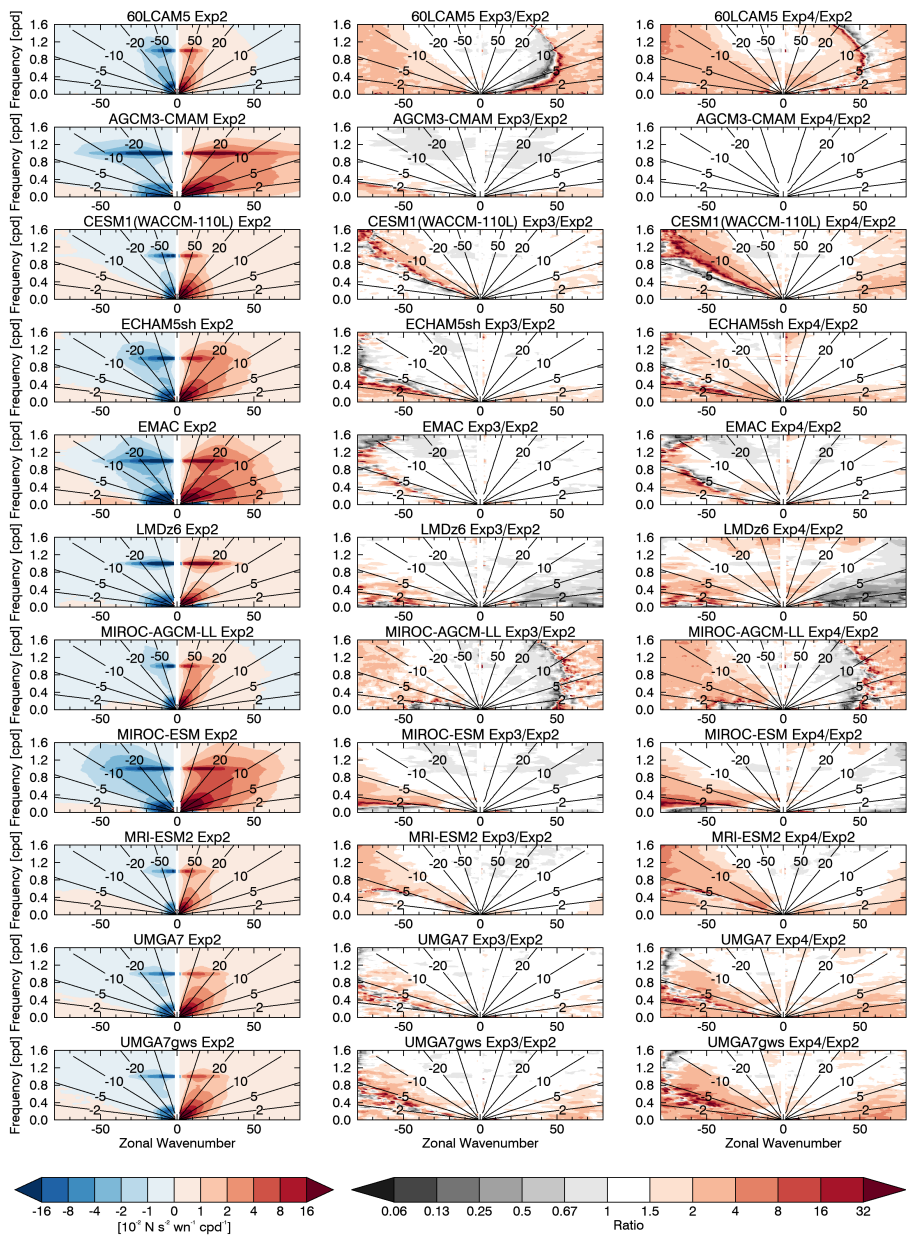


FIGURE 12 Vertical component of EP flux averaged between 85 and 70 hPa and 10°S and 10°N as a function of zonal wavenumber and frequency for Exp 2 (left column). Middle (right) column shows ratio of vertical EP flux for Exp 3 to Exp 2 (Exp 4 to Exp 2). Positive (negative) wavenumbers represent eastward (westward) propagating waves.

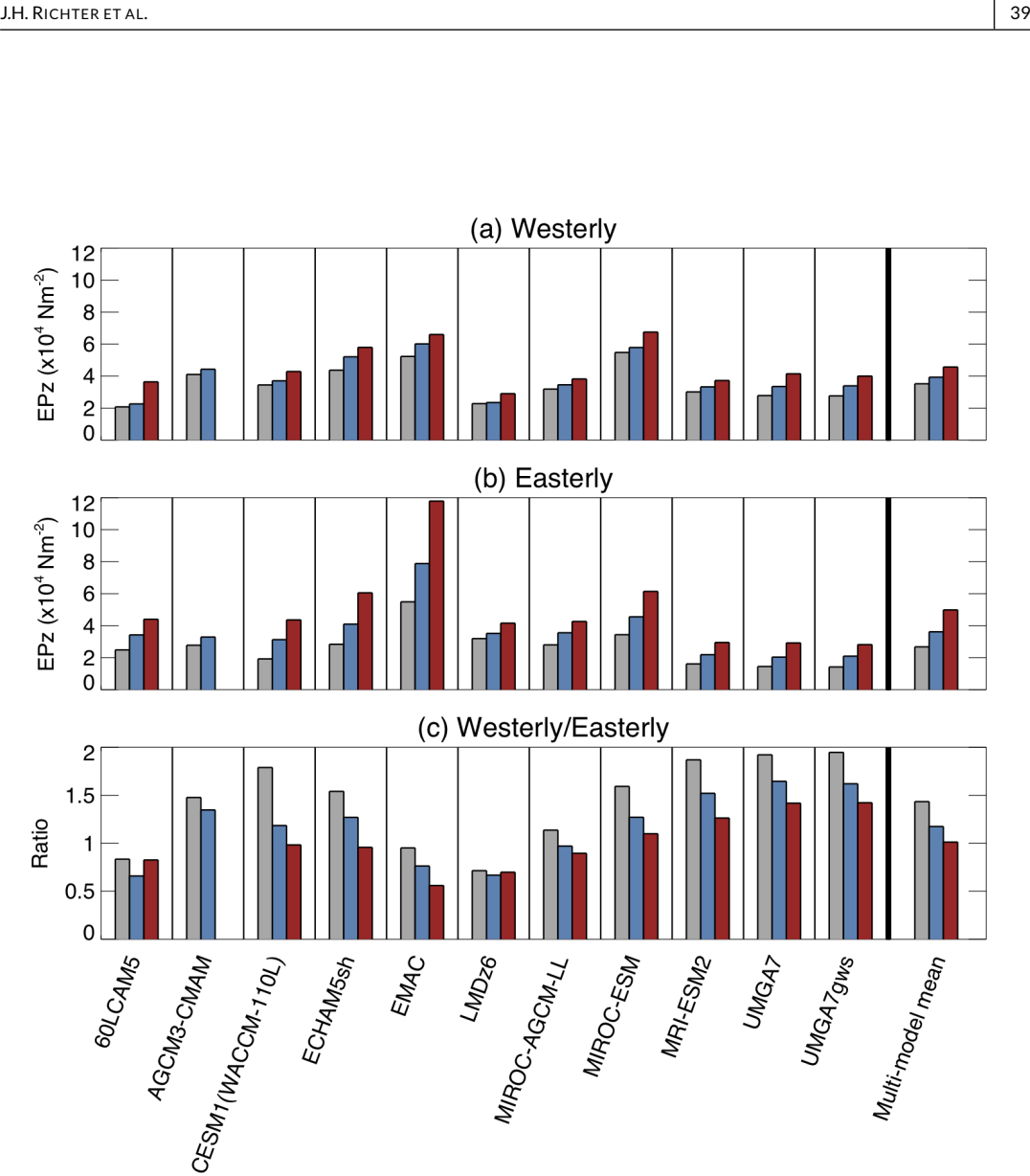


FIGURE 13 Vertical component of EP flux averaged between 85 and 70 hPa and over (a) westerly (negative) wave phase speeds, (b) easterly (positive) wave phase speeds. Ratio of westerly to easterly vertical component of EP flux is shown in panel (c). Values are shown for Exp 2 (gray), Exp 3 (blue) and Exp 4 (red) for individual models as well as the multi-model mean.

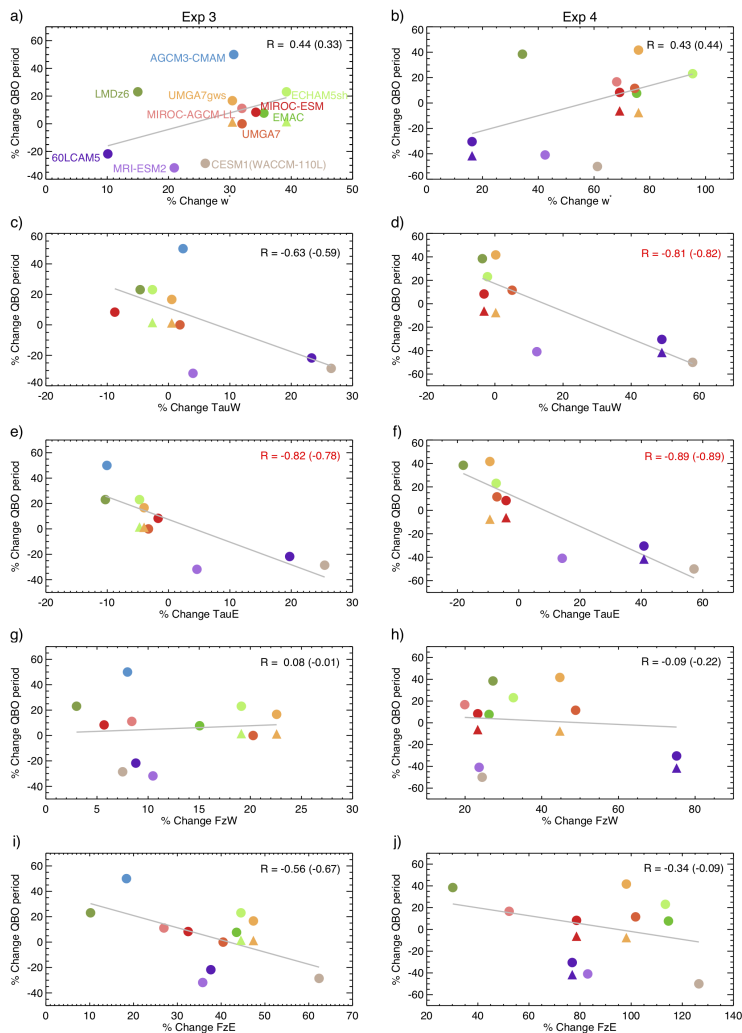


FIGURE 14 Scatter plot of relationship between changes in QBO period from Exp 3 to Exp 2 (left panels) and Exp 4 to Exp 2 (right panels) vs % change in \bar{w}^* averaged between 50 and 100 hPa (1st row); westerly (eastward) momentum flux at 100 hPa, TauW (2nd row); easterly (westward) momentum flux at 100 hPa, TauE (3rd row); westerly vertical component of EP flux averaged between 85 and 70 hPa, FzW (4th row); and easterly vertical component of EP Flux averaged between 85 and 70 hPa, FzE (5th row). Circles denote QBO period changes using the lag correlation method, and the grey line shows the correlation line using those values. Triangles depict QBO period changes calculated using the TT method and are only shown when the triangles don't overlap with the circles. Linear correlation coefficient, R, is depicted in the top right corner of the plot, with the first value showing correlations with QBO period changes derived using the lag correlation method and correlations with QBO period changes derived using the TT method are shown in parenthesis. Red color indicates that the correlation is significant according to a two-sided student t-test (p -value < 0.05). Model labels are in the top left panel. In the second and third rows EMAC and MIROC-AGCM-LL are missing as TauW/TauE were not available for EMAC and MIROC-AGCM-LL does not use a GW parameterization.

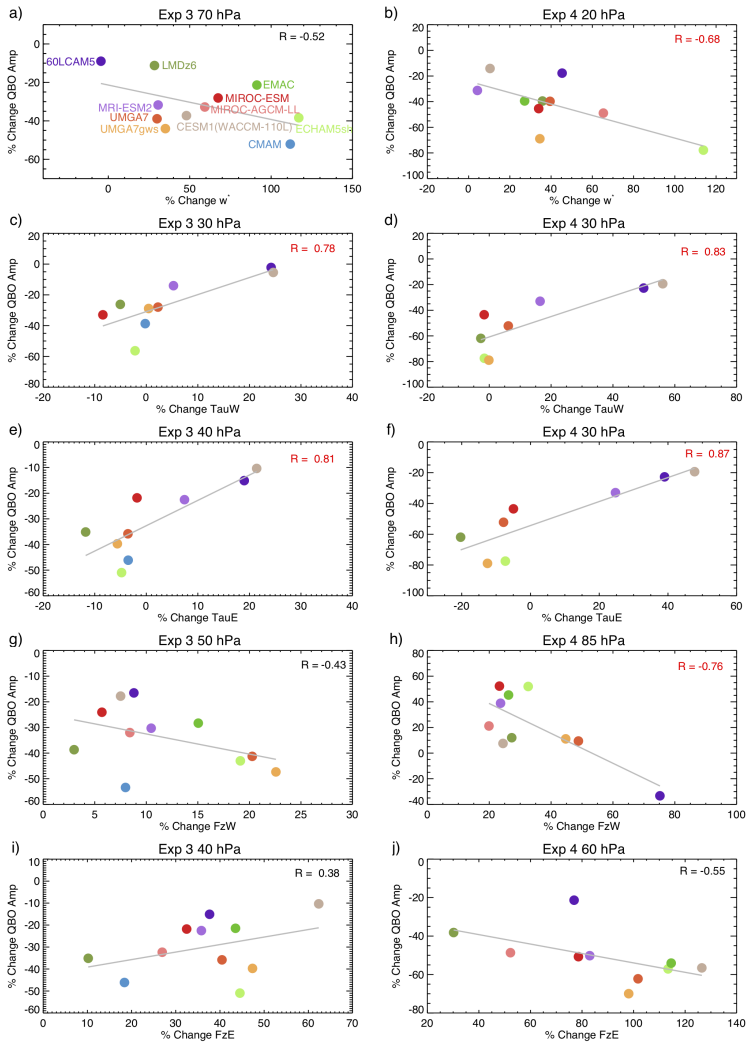
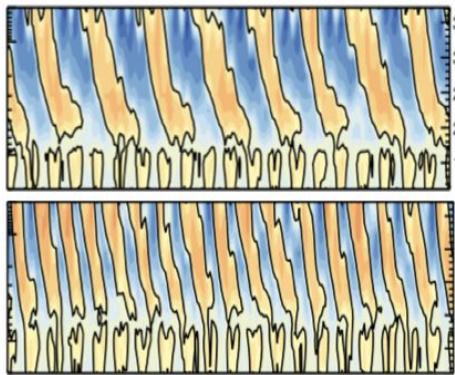


FIGURE 15 Scatter plot of relationship between changes in QBO amplitude from Exp 3 to Exp 2 (left panels) and Exp 4 to Exp 2 (right panels) vs: % change in w^* at the same level as QBO amplitude depicted in the panel title (top row); westerly (eastward) momentum flux at the same level as QBO amplitude, TauW, (2nd row); easterly (westward) momentum flux at the same level as QBO amplitude, TauE, (3rd row); westerly vertical component of EP flux averaged between 85 and 70 hPa (4th row); and easterly vertical component of EP flux averaged between 85 and 70 hPa (5th row). Correlations with amplitude are shown for the level at which maximum correlation exists. Model labels are shown in the top left panel. Linear correlation coefficient, R , is depicted in the top right corner of the plot. Red color indicates that the correlation is significant according to a two-sided student t -test (p -value < 0.05). In the 2nd and 3rd rows EMAC and MIROC-AGCM-LL are missing as TauW/TauE were not available for EMAC and MIROC-AGCM-LL does not use a GW parameterization.

Response of the quasi-biennial oscillation to a warming climate in global climate models

Jadwiga H. Richter*, Neal Butchart, Yoshio Kawatani, Andrew C. Bushell, Laura Holt, Federico Serva, James Anstey, Isla R. Simpson, Scott Osprey, Kevin Hamilton, Peter Braesicke, Chiara Cagnazzo, Chih-Chieh Chen, Rolando R. Garcia, Lesley J. Gray, Tobias Kerzenmacher, Francois Lott, Charles McLandress, Hiroaki Naoe, John Scinocca, Timothy N. Stockdale, Stefan Versick, Shingo Watanabe, Kohei Yoshida, Seiji Yukimoto



The response of the quasi-biennial oscillation (QBO) to a warming climate was examined in eleven general circulation models. No consistency was found among the models for the QBO period response. In contrast, all the models projected a decrease in the QBO amplitude in a warmer climate.